Title

MeCP2 isoform e1 mutant mice recapitulate motor and metabolic phenotypes of Rett syndrome

Journal

Human Molecular Genetics, 27(23)

ISSN

0964-6906

Authors

Ciernia, Annie Vogel
Yasui, Dag H
Pride, Michael C
et al.

Publication Date

2018-12-01

DOI

10.1093/hmg/ddy301

Peer reviewed

Human Molecular Genetics, 2018, Vol. 27, No. 23 4077–4093

doi: 10.1093/hmg/ddy301
Advance Access Publication Date: 21 August 2018
General Article

GENERAL ARTICLE

MeCP2 isoform e1 mutant mice recapitulate motor and metabolic phenotypes of Rett syndrome

Annie Vogel Ciernia[1,2,3], Dag H. Yasui[1], Michael C. Pride[3,4], Blythe Durbin-Johnson[5], Adriana B. Noronha[1], Alene Chang[1], Trina A. Knotts[6], Jennifer R. Rutkowsky[6], Jon J. Ramsey[6], Jacqueline N. Crawley[3,4,†] and Janine M. LaSalle[1,2,3,†,*]

[1]Department of Medical Microbiology and Immunology, UC Davis School of Medicine, University of California, Davis, CA, USA, [2]UC Davis Genome Center, University of California, Davis, CA, USA, [3]UC Davis MIND Institute, University of California, Davis, CA, USA, [4]Department of Psychiatry and Behavioral Sciences, UC Davis School of Medicine, University of California, Davis, CA, USA, [5]Department of Public Health Sciences, UC Davis School of Medicine, University of California, Davis, CA, USA and [6]Department of Molecular Biosciences, UC Davis School of Veterinary Medicine, University of California, Davis, CA, USA

*To whom correspondence should be addressed at: Medical Microbiology and Immunology, One Shields Ave. University of California, Davis, CA 95616, USA. Tel: +530 7547598; Email: jmlasalle@ucdavis.edu

Abstract

Mutations in the X-linked gene *MECP2* cause the majority of Rett syndrome (RTT) cases. Two differentially spliced isoforms of exons 1 and 2 (MeCP2-e1 and MeCP2-e2) contribute to the diverse functions of MeCP2, but only mutations in exon 1, not exon 2, are observed in RTT. We previously described an isoform-specific MeCP2-e1-deficient male mouse model of a human RTT mutation that lacks MeCP2-e1 while preserving expression of MeCP2-e2. However, RTT patients are heterozygous females that exhibit delayed and progressive symptom onset beginning in late infancy, including neurologic as well as metabolic, immune, respiratory and gastrointestinal phenotypes. Consequently, we conducted a longitudinal assessment of symptom development in MeCP2-e1 mutant females and males. A delayed and progressive onset of motor impairments was observed in both female and male MeCP2-e1 mutant mice, including hind limb clasping and motor deficits in gait and balance. Because these motor impairments were significantly impacted by age-dependent increases in body weight, we also investigated metabolic phenotypes at an early stage of disease progression. Both male and female MeCP2-e1 mutants exhibited significantly increased body fat compared to sex-matched wild-type littermates prior to weight differences. *Mecp2e1*$^{-/y}$ males exhibited significant metabolic phenotypes of hypoactivity, decreased energy expenditure, increased respiratory exchange ratio, but decreased food intake compared to wild-type. Untargeted analysis of lipid metabolites demonstrated a distinguishable profile in MeCP2-e1 female mutant liver characterized by increased triglycerides. Together, these results demonstrate that MeCP2-e1 mutation in mice of both sexes recapitulates early and progressive metabolic and motor phenotypes of human RTT.

[†]Co-senior authors.

Received: June 25, 2018. **Revised:** August 10, 2018. **Accepted:** August 14, 2018

Introduction

Mutations in the X-linked gene encoding methyl CpG-binding protein 2 (MeCP2) cause the majority of Rett syndrome (RTT) cases. The specific role for MeCP2 in the molecular pathogenesis of RTT is complex, involving multiple molecular mechanisms and cell types. MeCP2 has two alternatively spliced forms (MeCP2-e1 and MeCP2-e2), and mutations in *MECP2e1* (exon 1) but not *MECP2e2* (exon 2) have been linked to RTT. The two isoforms differ in their N-terminals by alterative inclusion of *Mecp2 exon 2* amino acids. MeCP2-e1 contains amino acids from exons 1, 3 and 4 while MeCP2-e2 contains amino acids encoded by all four exons but utilizes an alternative start codon in exon 2, resulting in the translation of only exons 2, 3 and 4 (1) (Fig. 1A). The vast majority of RTT mutations occur in *MECP2* exons 3 and 4; however, mutations in exon 1, but not exon 2, have been identified (1–3). MeCP2-e1 is the primary isoform expressed in the central nervous system (4) and has higher protein stability than MeCP2-e2 (5), further suggesting that MeCP2-e1 is the dominant isoform in brain. We recently demonstrated a critical role for MeCP2-e1 in the pathogenesis of RTT (5) by creating a novel mouse model based on an orthologous MeCP2-e1 translation start site mutation identified in patients with classic RTT (2,3) (*Mecp2e1*$^{-/y}$ mice) (Fig. 1A). This isoform-specific model lacks MeCP2-e1 translation while preserving expression of the MeCP2-e2 isoform, allowing for the examination of the specific function of MeCP2-e1. Male *Mecp2e1*$^{-/y}$ mice recapitulate many RTT-like neurologic deficits (5) including development of hind limb clasping, motor deficits and early lethality (5). These findings are in contrast to a mouse model with selective deletion of exon 2 that did not show neurologic symptoms (6). Together, the evidence suggests that MeCP2-e1 deficiency alone is sufficient to induce neurologic symptoms underlying RTT in male mice.

The majority of previous work on MeCP2 mouse models of RTT has focused on *Mecp2*$^{-/y}$ hemizygous male mice as they show early and progressive symptom onset and lethality. Previous work on female mouse models of RTT has focused primarily on heterozygous *Mecp2* mutations expressed in 20–40% of all cells (7,8). Initial characterization of heterozygous knockout females (*Mecp2*$^{tm1.1bird-/+}$) reported delayed phenotype development until 4–6 months of age (9,10). Recently, more detailed work in female heterozygous mouse models has revealed mixed findings for the age of phenotype development, depending on background strain and mutation type (11–16). However, to date there has been limited exploration of the time course of phenotype development and no behavioral characterization of isoform-specific manipulations of MeCP2 in female mouse models. Given that RTT occurs almost exclusively in females and there is no current effective treatment, there is a great need to develop a preclinical female mouse model of RTT that recapitulates the delayed behavioral phenotypes observed in human females with RTT.

While MeCP2 is most highly expressed in neurons, human female RTT patients exhibit immune, microbiome, mitochondrial and metabolic manifestations that are likely reactionary to the causal mutation and neuronal dysfunction (17–25). Metabolic dysfunctions are observed in RTT patients and mouse models, but whether these are consequences of inflammation or more directly mediated by *MECP2,* mutation is currently unknown. While RTT girls are generally not obese, perhaps due to the inability to self-feed, they have elevated morning leptin and adiponectin serum levels (17) as well as alterations in energy balance (26–28). Furthermore, RTT has significant commonalities with mitochondrial disorders, including elevated lactate and pyruvate in blood and cerebral spinal fluid (29), as well as markers of oxidative damage (30) that are also seen in mouse models (31,32). Lipid metabolism was identified in an unbiased screen for rescue of RTT mouse phenotypes (33) and was later shown to result in metabolic alterations in RTT mice (34). Metabolic or oxidative stress alterations have been modified in several therapeutic trials of RTT mouse models (20), with some discrepancies by strain and age (35,36). Since the most promising therapeutics for RTT target metabolic pathways (37), such as AKT/mTOR (38,39), oxidative stress (31,40) and lipid metabolism (33,41), it is imperative to characterize developmental, metabolic and motor phenotypes in female RTT mouse models.

To address the role of MeCP2-e1 in the development of phenotypes relevant to RTT, we performed a longitudinal assessment of *Mecp2e1*$^{-/+}$ females and *Mecp2e1*$^{-/y}$ male mice across development and into adulthood. We assessed developmental milestones during the first 3 weeks of life and monitored the progressive development of hind limb clasping and changes in body weight into adulthood. In addition, we performed assays examining anxiety, sociability, motor function, cognition and metabolism. A delayed and progressive onset of hind limb clasping, increased body weight and motor impairments was observed, reminiscent of the delayed symptom onset observed in females with RTT. Our findings indicate that changes in body weight and metabolism may exacerbate motor impairments in the *Mecp2e1*$^{-/+}$ female mice, suggesting that metabolic phenotypes may serve as a novel therapeutic avenue for RTT.

Results

Both female and male MeCP2-e1 mutant mice show an onset of hind limb-clasping phenotypes by 2 months that precede a progressive increase in body weight

To examine potential early phenotypes in *Mecp2e1*-deficient mice, a panel of developmental milestones was assessed across the first 21 days of life. The majority of measures showed no significant differences in mutant development compared to sex-matched wild-type littermates (Supplementary Material, Table S1). The two exceptions were slight delays in pinnae detachment in *Mecp2e1*$^{-/+}$ females and cliff avoidance in *Mecp2e1*$^{-/y}$ males. However, all other measures were indistinguishable from wild-type, indicating normal pre-weaning development in mutant animals.

Post-weaning body weight and hind limb clasping scores were assessed weekly and showed progressive symptom development in both male and female mutants (Fig. 2 and Supplementary Material, Table S2). Female *Mecp2e1*$^{-/+}$ mice showed clasping scores that were significantly different from wild-type beginning at postnatal day (PND) 52 that progressed, then stabilized after PND 69. This neurologically based hind limb-clasping phenotype in *Mecp2e1*$^{-/+}$ females preceded a progressive significant increase in body weight starting at PND 74. *Mecp2e1*$^{-/y}$ male mice showed a similar but slightly delayed onset of significant differences from wild-type in hind limb clasping by PND 61 and significantly higher body weights beginning at PND 92. The hind limb-clasping phenotype was more severe in male compared to female mutants, but increases in body weight relative to wild-type littermates were similar in magnitude between sexes.

Both female and male mutant mice (PND 46 and 53) showed increased time in the open arm of the elevated plus maze (Supplementary Material, Figs. S1 and S2) as previously found for MeCP2e1$^{-/y}$ males (42) and *Mecp2*$^{tm1.1bird-/+}$ females (16) at similar ages. There were no significant differences between genotypes for the number of transitions between arms indicating the

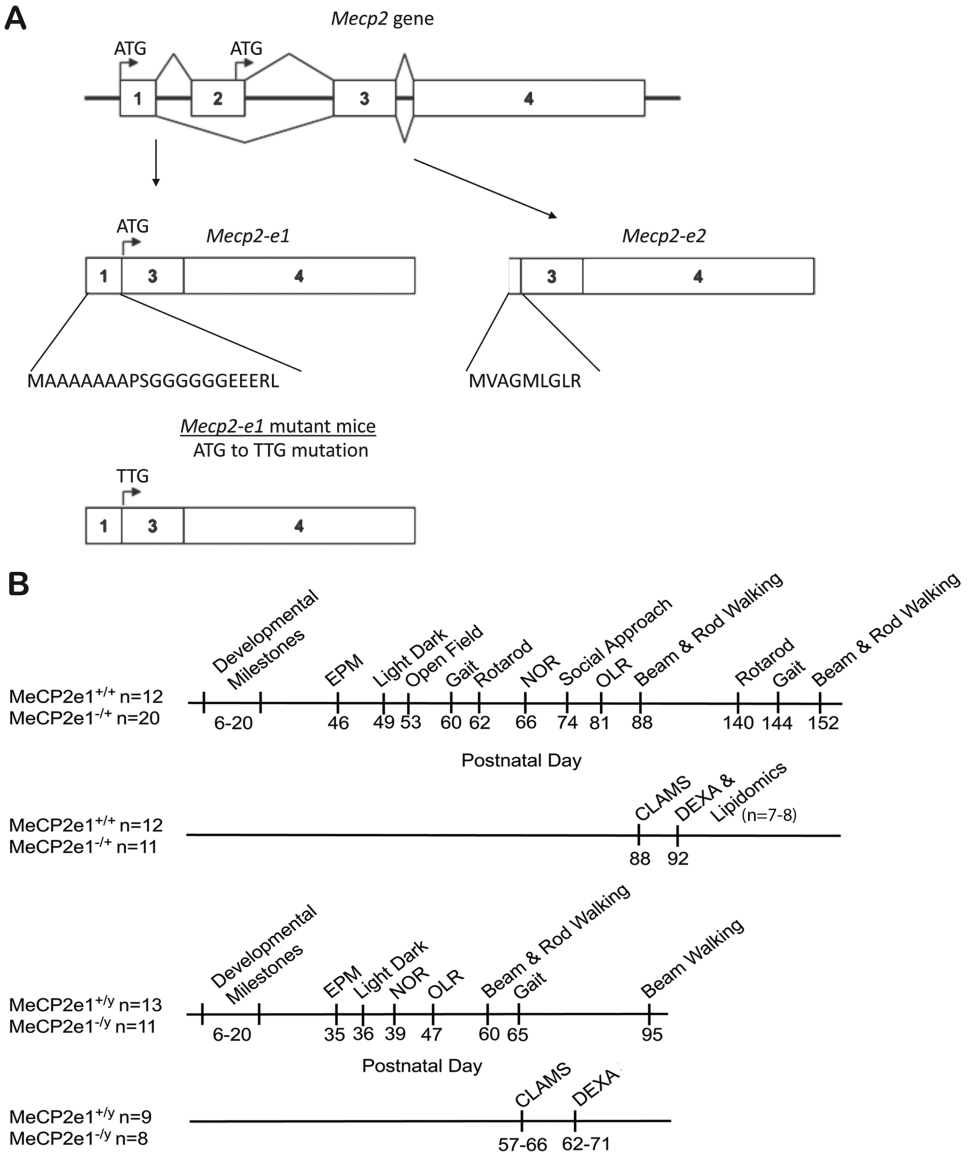

Figure 1. MeCP2-e1 isoform splicing and experimental design. **(A)** The *Mecp2* transcript is alternatively spliced into the e1 and e1 isoforms with different N-terminals (amino acid sequence listed). MeCP2-e1 mutant mice have a single-nucleotide substitution that results in a loss of the start codon (ATG–TTG mutation) and no translation of the MeCP2-e1 protein. The MeCP2-e2 isoform is still transcribed and translated. **(B)** The timeline for behavioral, CLAMS, DEXA and lipidomics analysis of MeCP2e1 mutant females (*Mecp2e1*$^{-/+}$) and wild-type littermates (*MeCP2e1*$^{+/+}$) and mutant males (*MeCP2e1*$^{-/y}$) and wild-type littermates (*MeCP2e1*$^{+/y}$).

increased time in the open arm was not due to changes in motor function. Female *Mecp2e1*$^{-/+}$ mice did not differ from wild-type littermates in the light–dark exploration task (Supplementary Material, Fig. S1); however, *Mecp2e1*$^{-/y}$ males did spend significantly less time in the dark chamber than wild-type littermates with no difference in the number of transitions (Supplementary Material, Fig. S2). The inconsistent findings on the two measures of anxiety indicate potential abnormalities in more subtle aspects of the two tasks and are consistent with previously observed discrepancies between phenotypes on the two tasks for *Mecp2*$^{tm1.1bird-/+}$ females (16). There were no significant differences between mutant and wild-type females in the open field text of exploratory behaviors except in the measure of center time, where *Mecp2e1*$^{-/+}$ mice spent significantly less time in the center of the arena than wild-type littermates (Supplementary Material, Fig. S3). Adding body weight as a covariate did not alter the results in these tasks (Supplementary Material, Tables S3 and S4).

Female MeCP2-e1 mutant mice exhibit early motor deficits impacted by age-related body weight differences

Motor function was assessed using several different tasks including analysis of gait-, beam- and rod-walking latency and accelerating rotarod performance. Female *Mecp2e1*$^{-/+}$ mice showed significant impairments on several measures of gait performance (Fig. 3). At PND 60, mutant females showed significant impairments in stride length, hind base and paw separation. However, by PND 144 only the differences in stride length were significant. Body weight was a significant covariate for the

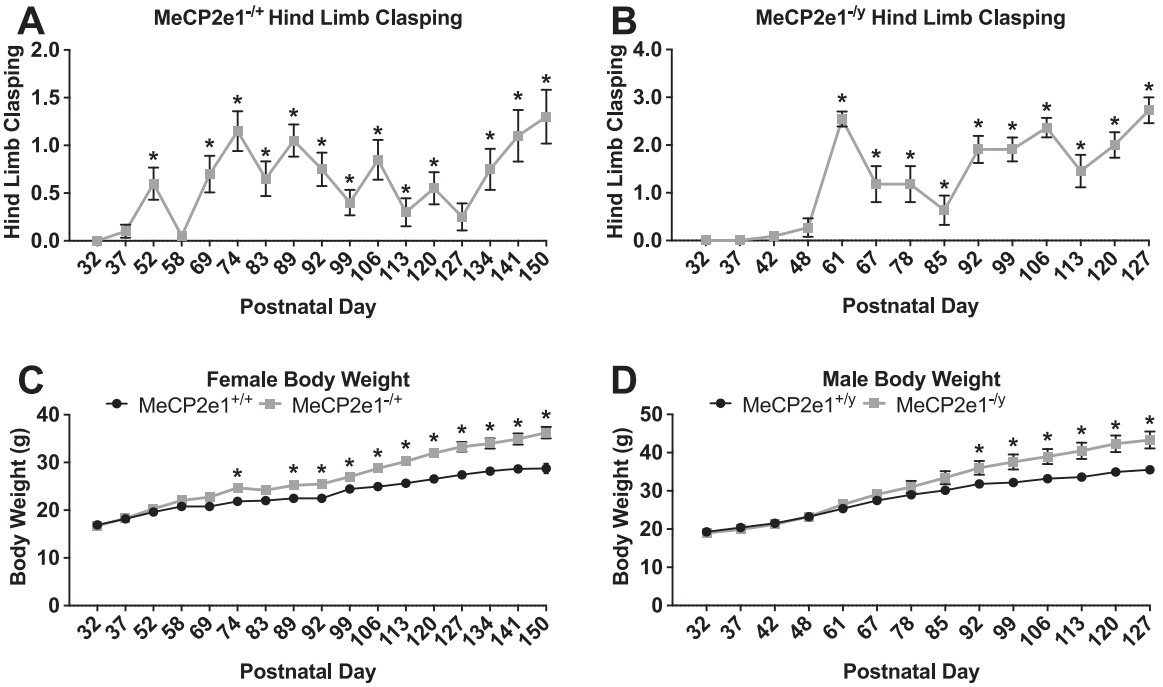

Figure 2. Symptom development across age in male and female MeCP2e1 mutant mice. Hind limb clasping was assessed weekly using a rating scale from 0 (no clasping) to 5 (severe). Data were analyzed using an exact binomial test that tests whether there were significantly more mutant animals with clasping scores > 0 for each time point (PND). *P*-values were Benjamini–Hochberg corrected across time points. **(A)** Hind limb clasping in females. **(B)** Hind limb clasping in males. Body weight (grams) was taken weekly across development and analyzed by linear mixed effects model (see methods) and Benjamini–Hochberg corrected comparisons were conducted between genotypes for each PND. **(C)** Body weight in females. **(D)** Body weight in males. * mutant versus wild-type corrected *P*-value < 0.05, statistical tests are shown in detail in Supplementary Material Table S2. Mean +/− standard error of the mean (SEM).

measure of stride length but did not alter the significance of the effect of genotype (Supplementary Material, Table S3). Adding body weight as a covariate did alter the main effect of genotype for the measure of hind base, indicating that this measure of gait may be more sensitive to weight changes. *Mecp2e1*$^{-/y}$ males did not show any significant difference from wild-type littermates on any of the gait measures (Supplementary Material, Fig. S4 and Table S4).

Female *Mecp2e1*$^{-/+}$ mice showed significant impairments in beam walking at both PND 88 and 152 (Fig. 4 and Supplementary Material, Table S3). Deficits were specific to the smallest diameter beam (beam 3) at the younger time point and to the widest diameter beam (beam 1) at the older time point, potentially representing impairments in different aspects of the task with symptom progression. This task was also sensitive to alterations in body weight. When added as a covariate, the main effect of genotype was no longer significant at either time point, indicating that increased body weight in the mutant females is a significant contributor to impairments in this task. In comparison, female mutant mice did not show any significant impairment on rod walking (Supplementary Material, Fig. S5 and Table S3). Female *Mecp2e1*$^{-/+}$ mice did show progressive impairments in the accelerating rotarod (Fig. 4 and Supplementary Material, Table S3). At PND 62, performance between wild-type and mutant females was equivalent across all 3 days of training, indicating normal motor performance and learning. At PND 140, *Mecp2e1*$^{-/+}$ mice showed significant impairments across all 3 days of training. The impairments at PND140 were sensitive to changes in body weight. When body weight was included as a covariate, the main effect of genotype was no longer significant indicating that at least a portion of the impairment in performance was due to increased weight in the mutants. Motor and phenotypic symptoms were also delayed relative to those observed in heterozygous whole exon deletion female models (16), suggesting that some MeCP2e-1 roles in motor skills may be compensated for by MeCP2-e2.

Male *Mecp2-e1*$^{-/y}$ mice also showed significant impairments on the beam-walking but not rod-walking task (Supplementary Material, Fig. S6 and Table S4). At PND 60, *Mecp2e1*$^{-/y}$ mice showed significant impairments relative to wild-type littermates on the smallest diameter beam (beam 3). At PND 95, *Mecp2e1*$^{-/y}$ mice were significantly impaired on all three diameter beams. At the PND 60 but not PND 95, adding body weight as a covariate resulted in a loss of the significant genotype effect. This suggests that the impairments at the earlier time point may be driven by body weight but that later impairments are largely motor in origin.

Lack of significant deficits in sociability or short-term memory in young female MeCP2-e1 mutant mice

Male *Mecp2e1*$^{-/y}$ mice were previously shown to have deficits in social behavior (5) and consequently, we examined sociability of female *Mecp2e1*$^{-/+}$ mice in the three-chambered social approach task (Supplementary Material, Fig. S7). *Mecp2e1*$^{-/+}$ mice performed similarly to wild-type littermates in the number of transitions between chambers during both the habituation and testing phases, indicating that any motor impairments minimally impacted the task. Both *Mecp2e1*$^{-/+}$ mice and wild-type littermates showed significant preferences for the novel mouse over the novel object both in chamber time and sniff time. Together, this suggests that female *Mecp2e1*$^{-/+}$ mice do not have impairments in sociability at PND 74.

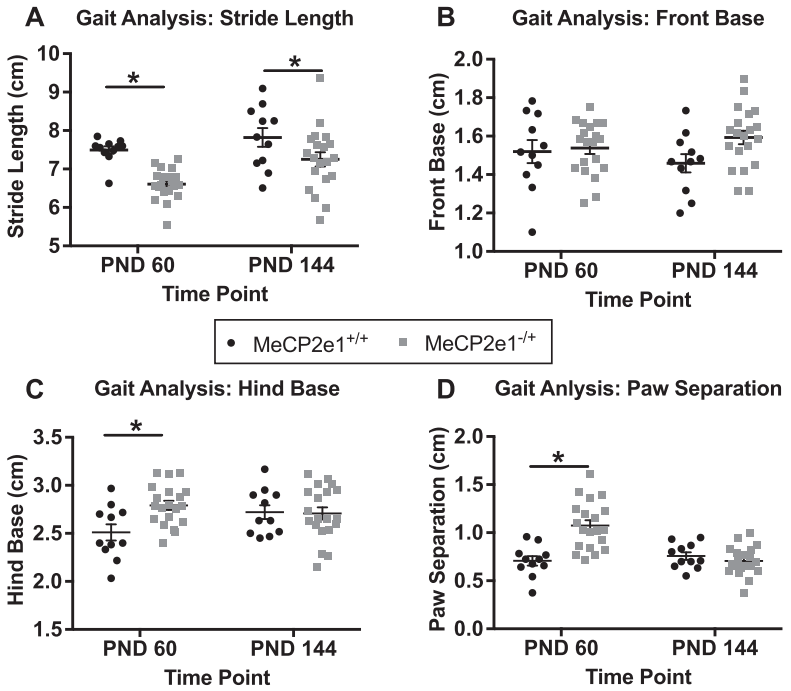

Figure 3. Female mutant mice show impairments in gait in early development. **(A)** *Mecp2e1*$^{-/+}$ mice show decreased stride length at both PND 60 and 144. Impairments measures of front base (**B**), hind base (**C**) and paw separation (**D**) only were significantly altered at PND 60. Mean +/− SEM. * $P < 0.05$ Benjamini–Hochberg corrected comparisons between genotypes, statistical tests shown in detail in Supplementary Material, Table S3.

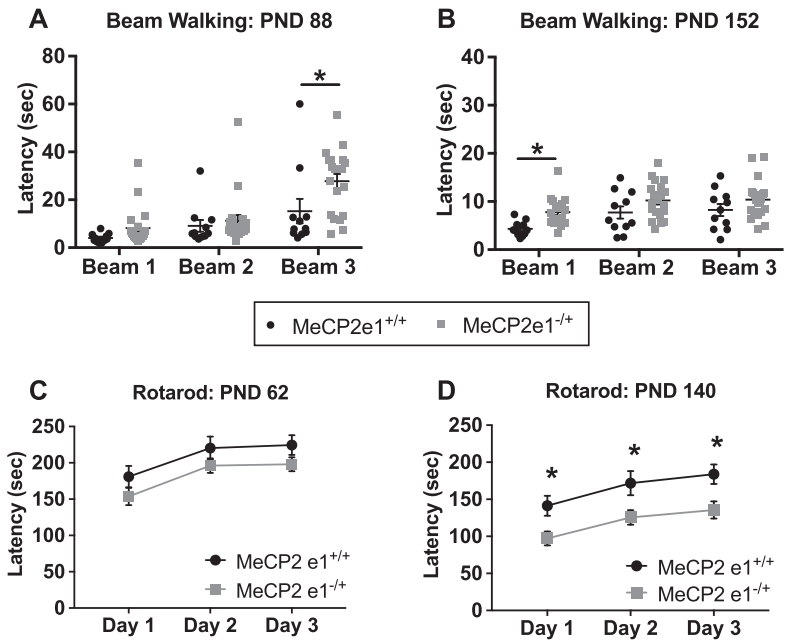

Figure 4. Female mutant mice show impairments in motor tasks. **(A)** *Mecp2e1*$^{-/+}$ mice show increased latency to transverse beam 3 (smallest diameter) at PND 88. **(B)** *Mecp2e1*$^{-/+}$ mice show increased latency to transverse beam 1 (largest diameter) at PND 152. **(C)** *Mecp2e1*$^{-/+}$ mice show similar performance to wild-type littermates on the accelerating rotarod across 3 days of training at PND 62. **(D)** *Mecp2e1*$^{-/+}$ mice show a decreased ability to remain on the accelerating rotarod (shorter latency) compared to wild-type littermates across 3 days of training at PND 140. Mean +/− SEM. * $P < 0.05$ Benjamini–Hochberg corrected comparisons between genotypes, statistical tests shown in detail in Supplementary Material, Table S3.

Both male and female mutant mice were examined for cognitive performance using the short-term memory version of the novel object task and novel location task (43). Both *Mecp2e1*$^{-/+}$ and wild-type female mice showed a significant preference for the novel object over the familiar object and there were no differences in total exploration time or distance traveled at training or testing (Supplementary Material, Fig. S8 and Table S3). For the object location version of the task, *Mecp2e1*$^{-/+}$ mice showed a significant preference for the object in the new location and wild-type littermates showed a marginally significant ($P < 0.06$) preference. There was no difference between genotypes for total exploration at training or testing and no difference in total

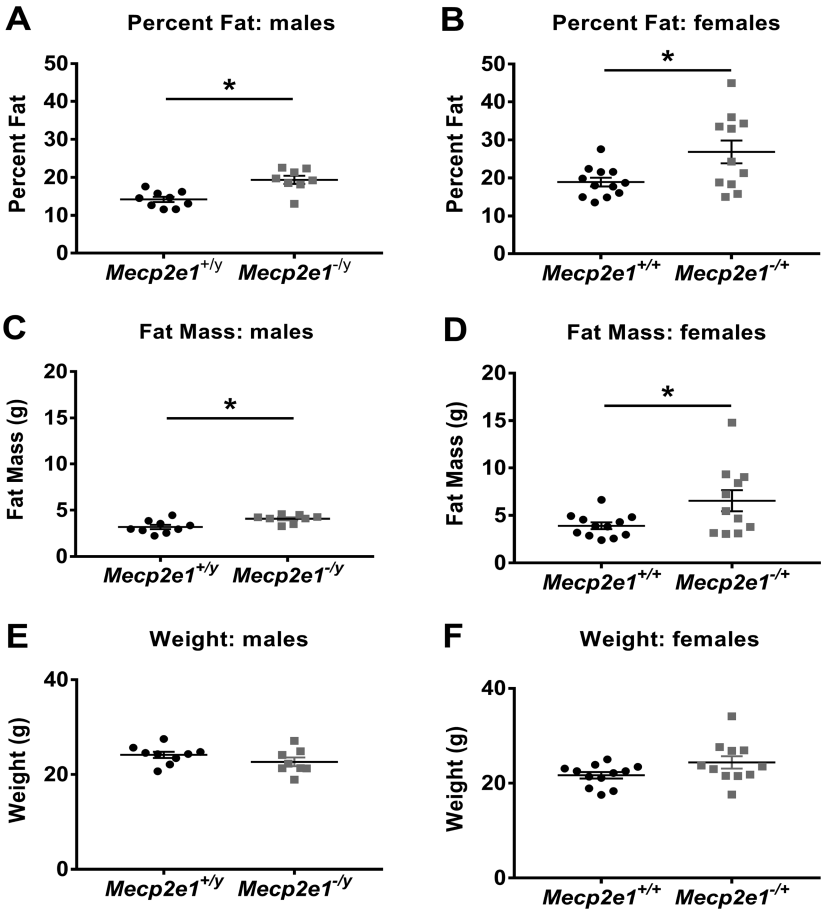

Figure 5. DEXA analysis reveals body composition alterations for *Mecp2e1* mutant mice. For these studies, *Mecp2e1*$^{+/y}$ (N = 9), *Mecp2e1*$^{-/y}$ (N = 8) (PND 62–71), *Mecp2e1*$^{-/+}$ (N = 11) and *Mecp2e1*$^{+/+}$ (N = 12) (PND 92) were analyzed. **(A)** A significant (P = 0.00096) elevation for percent fat in *Mecp2e1*$^{-/y}$ compared to control *Mecp2e1*$^{-/}$ mice is shown. **(B)** A significant (P = 0.0183) elevation in percent fat for *Mecp2e1*$^{-/+}$ compared to control *Mecp2e1*$^{+/+}$ littermates. **(C)** Fat mass in grams is elevated in *Mecp2e1*$^{-/y}$ (P = 0.028) and **(D)** *Mecp2e1*$^{-/+}$ (P = 0.0077) compared to *Mecp2e1*$^{+/y}$ and *Mecp2e1*$^{+/+}$ control littermates, respectively. **(E)** Weights are comparable between *Mecp2e1*$^{+/y}$ and *Mecp2e1*$^{-/y}$ mice (P = 0.2). **(F)** *Mecp2e1*$^{+/+}$ and *Mecp2e1*$^{-/+}$ mice have similar weights at the time of DEXA (P = 0.07). P-values were computed using an unpaired, two-tailed student's *t*-test. * = P-value < 0.050. Error bars correspond to SEM.

distance traveled. Together, these findings indicate intact short-term memory for both novel objects and object locations in *Mecp2e1*$^{-/+}$ mice. Similarly, both male wild-type and *Mecp2e1*$^{-/y}$ mice showed a significant preference for the novel compared to familiar object during novel object recognition testing (Supplementary Material, Fig. S8 and Table S4). However, *Mecp2e1*$^{-/y}$ mice did show significantly lower overall exploration during training and higher exploration during testing compared to wild-type littermates. For the object location version of the task, wild-type males showed a significant preference for the object in the new location and *Mecp2e1*$^{-/y}$ mice showed a marginally significant preference ($P < 0.06$). Again, *Mecp2e1*$^{-/y}$ mice showed higher overall exploration of the objects during training but not during testing. Overall, these findings suggest intact learning and short-term memory in both male and female mutant mice.

MeCP2e1 mutant males exhibit significantly increased body fat despite reduced food intake due to genotype effects on energy expenditure

Since previous studies suggest metabolic defects occur in both RTT females and *Mecp2*/MeCP2-deficient mouse models (20,31,34,44) and because of the progressive elevated body weight in MeCP2-e1 mutant mice, we sought to better characterize the metabolic phenotypes at an early stage of disease progression (PND 57–66 in males and PND 88–92 in females) when no significant differences in body weight were observed by analysis of variance (ANOVA) for this cohort (Supplementary Material, Fig. S10). Dual-energy X-ray absorptiometry (DEXA) was performed to measure fat mass and bone mineral density (BMD) and area. DEXA scans revealed that both *Mecp2e1*$^{-/y}$ males and *Mecp2e1*$^{-/+}$ females had elevated percent fat (Fig. 5A and B) and elevated fat mass (Fig. 5C and D). *Mecp2e1*$^{-/y}$ mice had elevated percent fat and fat mass compared to wild-type male littermates, and *Mecp2e1*$^{-/+}$ mice had elevated percent fat and fat mass compared to wild-type female littermates. These differences in *Mecp2e1*-deficient mice were surprising as weights were similar between *Mecp2e1*$^{-/y}$ and controls (Fig. 5E) as well between *Mecp2e1*$^{-/+}$ and control females (Fig. 5F). The results are consistent with genotype altering nutrient partitioning and inducing a shift in body composition independent of changes in body weight. DEXA analysis also revealed that *Mecp2e1*$^{-/y}$ males but not *Mecp2e1*$^{-/+}$ females had reductions in bone mineral content (BMC) (Supplementary Material, Fig. S12A and B), bone area (Supplementary Material, Fig. S12C and D) and body length (Supplementary Material, Fig. S12E and F).

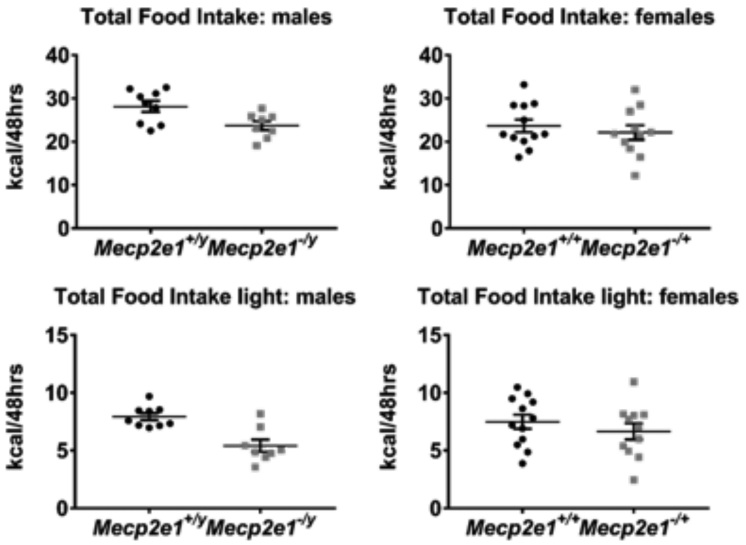

Figure 6. *Mecp2e1*$^{-/y}$ mice consume less calories during the light phase. (**A**) A significant ($P = 0.0173$) reduction for total cumulative food intake for 48 h represented as kilocalories per 48 h (kcal/48 h) between *Mecp2e1*$^{+/y}$ control and *Mecp2e1*$^{-/y}$ groups is shown. (**B**) Total cumulative food intake is comparable between *Mecp2e1*$^{-/+}$ and *Mecp2e1*$^{+/+}$ control littermates. (**C**) Sum food intake during the light phase reveals a significant reduction ($P = 0.0007$) in *Mecp2e1*$^{-/y}$ compared to *Mecp2e1*$^{+/y}$ littermate controls. (**D**) Sum food intake in the light phase is similar in *Mecp2e1*$^{-/+}$ and *Mecp2e1*$^{+/+}$ control littermates. For these studies, *Mecp2e1*$^{+/y}$ (N = 9), *Mecp2e1*$^{-/y}$ (N = 8), *Mecp2e1*$^{-/+}$(N = 11) and *Mecp2e1*$^{+/+}$ (N = 12) were analyzed. *P*-values were computed using an unpaired, two-tailed student's t-test. * $P < 0.05$.

To identify potential causes of the increased fat mass and progressive increase in body weights, food intake, energy expenditure, respiratory exchange ratio (RER) and physical activity of *Mecp2e1*-deficient mice were measured using a Comprehensive Lab Animal Monitoring System (CLAMS). Interestingly, despite having increased fat, *Mecp2e1*$^{-/y}$ mice consumed significantly less calories than *Mecp2e1*$^{+/y}$ wild-type male littermates (Fig. 6A) and this was driven primarily by significantly reduced consumption during the light phase (Fig. 6C). In contrast, *Mecp2e1*$^{-/+}$ females did not show significant effects on food consumption overall or during the light phase (Fig. 6B and D). Food consumption in the dark phase was not significantly different between *Mecp2e1*$^{+/y}$ and *Mecp2e1*$^{-/y}$ mice (Supplementary Material, Fig. S13A) nor between *Mecp2e1*$^{+/+}$ and *Mecp2e1*$^{-/+}$ females (Supplementary Material, Fig. S13B).

To determine the relationship between metabolism and physical activity, the total number of X-axis and X-axis ambulatory beam breaks was compared across *Mecp2e1* genotypes (Fig. 7). *Mecp2e1*$^{-/y}$ males showed reduced locomotion compared to wild-type littermates as shown by significant reductions in X-axis beam breaks (Fig. 7A) and X-axis ambulation (Fig. 7C). *Mecp2e1*$^{-/+}$ females showed a trend towards lower levels of activity, although the effect was not significant (Fig. 7B and D). The overall reduction in *Mecp2e1*$^{-/y}$ activity was due to reduced X-axis total activity and X-axis ambulation during the dark cycle (Supplementary Material, Fig. S14A and S14C). In contrast, *Mecp2e1*$^{-/+}$ females had normal X-axis total activity and X-axis ambulation during the dark cycle (Supplementary Material, Fig. S14B and S14D).

RER and energy expenditure were also examined as a possible explanation for the increased fat and body weights of MeCP2-e1 mutant mice. *Mecp2e1*$^{-/y}$ mice exhibited significantly increased RER (Fig. 8A), representing a shift towards increased carbohydrate oxidation compared to wild-type male littermates. Energy expenditure was also significantly lower in *Mecp2e1*$^{-/y}$ mice compared to control males (Fig. 8C), while *Mecp2e1*$^{-/+}$ females were not significantly different than female controls by either measurement (Fig. 8B and 8D). Analysis of covariance (ANCOVA) normalizing for either body weight ($P = 0.006482$) or lean mass ($P = 0.01526$) confirmed the reduction energy expenditure in *Mecp2e1*$^{-/y}$ males. In contrast, energy expenditure did not differ in *Mecp2e1*$^{-/+}$ females with either body weight ($P = 0.2257$) or lean mass ($P = 0.5225$) normalization by ANCOVA (Supplementary Material, Table S5). Interestingly, the alterations in RER and energy expenditure in *Mecp2e1*$^{-/y}$ males were primarily observed in the dark phase (6 p.m.–6 a.m.) of the circadian cycle (Supplementary Material, Fig.15A and 15C), although RER was not altered in the light phase when energy expenditure was also reduced (Supplementary Material, Fig. S16A and S16C). *Mecp2e1*$^{-/+}$ females did not differ from controls in RER and energy expenditure during the dark phase (Supplementary Material, Fig. S15B and S15D) as well as the light phase (Supplementary Material, Fig. S16B and S16D). Together, these results demonstrate a significant genotype effect of fuel usage and energy expenditure in the active dark hours that, together with reduced activity, appear to predispose MeCP2-e1-deficient male mice to lipid accumulation and weight gain despite reduced food intake.

MeCP2-e1 mutant female profiling of liver lipids demonstrates a distinct profile of triglycerides

Previous analysis of MeCP2 null *Mecp2*$^{-/y}$ liver has shown grossly elevated accumulation of triglyceride and cholesterol compared to control liver (34). Therefore, as *Mecp2e1*$^{-/+}$ females showed significant increases in fat mass compared to controls, we explored possible changes in lipid accumulation in livers from mutant females. Untargeted lipid profiling by mass spectrographic analysis was performed on *Mecp2e1*$^{-/+}$ and wild-type *Mecp2e1*$^{+/+}$ liver samples following CLAMS and DEXA analysis of the same animals. Relative lipid abundance from liver was determined by peak height compared to standards and analyzed using MetaboAnalyst 4.0 statistical analysis package. Figure 9A demonstrates that *Mecp2e1*$^{-/+}$ liver samples could be separated from wild-type female control liver samples in a partial least squares discriminant analysis (PLS-DA) of

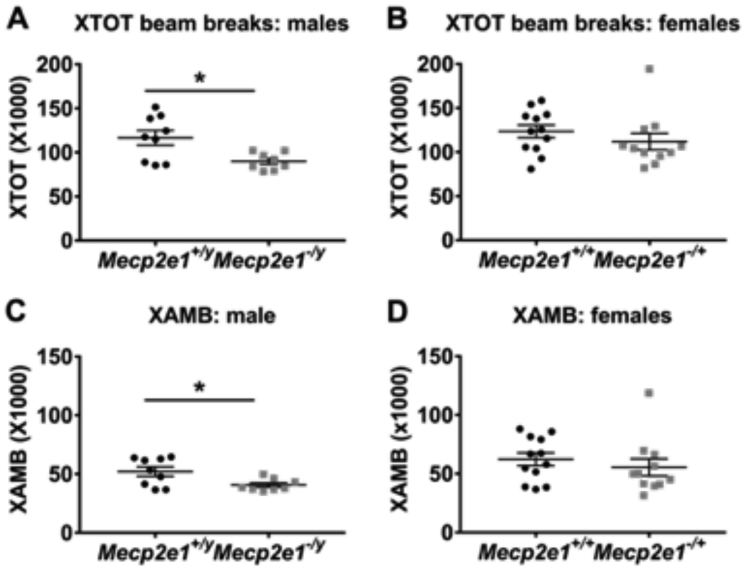

Figure 7. *Mecp2e1*$^{-/y}$ mice show reduced locomotion. **(A)** A significant ($P = 0.023$) reduction for total 48 h cumulative X beam breaks between *Mecp2e1*$^{+/y}$ control and *Mecp2e1*$^{-/y}$ groups is shown. **(B)** Total 48 h cumulative X beam breaks show a trend toward reduction in *Mecp2e1*$^{-/+}$ compared to *Mecp2e1*$^{+/+}$ controls. **(C)** Total 48 h cumulative X beam break analysis reveals a significant reduction ($P = 0.013$) in *Mecp2e1*$^{-/y}$ mice compared to *Mecp2e1*$^{+/y}$ control littermates. **(D)** A trend toward reduction in total 48 h X ambulation in *Mecp2e1*$^{-/+}$ mice compared to *Mecp2e1*$^{+/+}$ controls is observed. For these studies, *Mecp2e1*$^{+/y}$ (N = 9), *Mecp2e1*$^{-/y}$ (N = 8), *Mecp2e1*$^{-/+}$ (N = 11) and *Mecp2e1*$^{+/+}$ (N = 12) were analyzed. *P*-values were computed using an unpaired, two-tailed student's t-test. * $P < 0.05$.

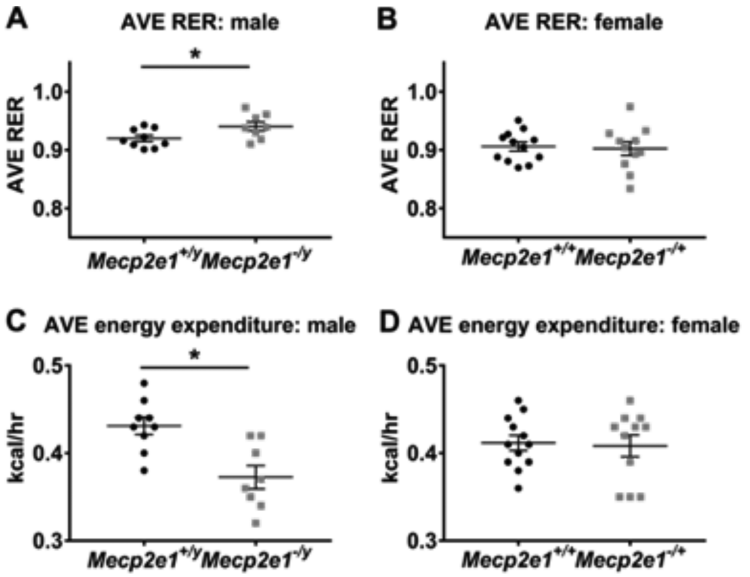

Figure 8. *Mecp2e1*$^{-/y}$ mice have elevated RER and reduced energy expenditure. **(A)** Average RER (AVE RER) shows elevation ($P = 0.0368$) in *Mecp2e1*$^{-/y}$ (N = 8) compared to littermate controls *Mecp2e1*$^{+/y}$ (N = 9). **(B)** AVE RER is similar between *Mecp2e1*$^{-/+}$ (N = 11) and *Mecp2e1*$^{+/+}$ (N = 12) control littermates. **(C)** Average energy expenditure (AVE Heat) for *Mecp2e1*$^{-/y}$ mice (N = 8) is significantly reduced ($P = 0.00194$) compared to controls *Mecp2e1*$^{+/y}$ (N = 9). **(D)** Average energy expenditure was similar between *Mecp2e1*$^{+/+}$ control (N = 12) and *Mec2pe1*$^{-/+}$ (N = 11) mice. *P*-values were computed using an unpaired, two-tailed student's t-test. * $P < 0.05$.

lipid abundance. Several individual lipids were significantly increased by raw P-values, although none were significant after false discovery rate (FDR) correction (Fig. 9B). Of the top lipid differences ranked by raw *P*-values, triglycerides 547, 542, 565 and 512 were elevated (Fig. 9C). Together, these results suggest that *Mecp2e1*$^{-/+}$ female mice have elevated triglycerides compared to their wild-type littermates.

Discussion

Mutations in *MECP2* cause the majority of RTT cases and despite many years of research, we still have a limited understanding of how MeCP2 causes a regressive disease phenotype in heterozygous and mosaic females. Furthermore, there has been limited progress on how each isoform of MeCP2 (MeCP2-e1 and -e2) contributes to the diverse functions of MeCP2. This study provides some important novel findings about the specific role of MeCP2-e1 deficiency on disease progression, with a specific focus on the female phenotypes that are expected to be most important to understanding the complex pathogenesis of human RTT. First, we demonstrate that female MeCP2-e1-deficient mice show hind-clasping phenotypes at the same stage as male MeCP2-e1-deficient littermates, around 2 months of age. Second, both male and female MeCP2-e1-deficient mice exhibit

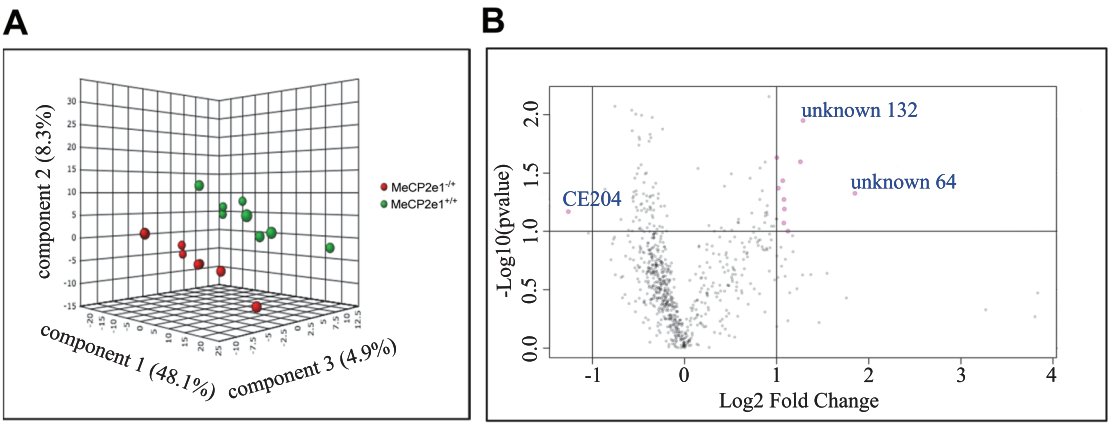

C

Lipid	FC	log2(FC)	raw.pval	LOG10(p)
unknown 132	2.4385	1.286	0.011233	1.9495
Triglyceride 547/182/182,183	2.0018	1.0013	0.023354	1.6316
unknown 56	2.391	1.2576	0.02533	1.5964
M1 Isotope of Triglyceride 542	2.0935	1.0659	0.036779	1.4344
unknown 145	2.0258	1.0185	0.042674	1.3698
unknown 64	3.6038	1.8495	0.047228	1.3258
Triglyceride 565/160/181/224	2.113	1.0793	0.053263	1.2736
unknown 301	2.1194	1.0837	0.06431	1.1917
Cholesterol ester 204	0.4169	-1.2624	0.067732	1.1692
Triglyceride 512	2.11	1.0772	0.084759	1.0718
unknown 289	2.1767	1.1221	0.099659	1.0015

Figure 9. Untargeted lipid profiling analyses of *Mecp2e1*$^{-/+}$ liver indicate elevated triglycerides. **(A) PLS-DA** shows a clear separation between *Mecp2e1*$^{-/+}$ samples (green, N = 8) and control littermate *Mecp2e1*$^{+/+}$ (red, N = 7) female liver samples based on untargeted lipid profiling. **(B)** A volcano plot of fold change (FC) (X axis) and raw P-values of genotype differences based on lipid abundance determined by mass spectroscopic analysis. Pink circles represent lipids with a log2 FC > 1.0 and a top raw P-values rank, with the identities of the know lipids shown in **(C)**. Of the known lipids, triglycerides were the most represented category of lipids that had elevated abundance in *Mecp2e1*$^{-/+}$ liver samples compared to control liver samples.

significant and progressive weight gain, but at a time point later than significant differences in hind limb clasping, fat mass and metabolism were observed. Third, female MeCP2-e1-deficient mice exhibit significant motor deficits at early stages of disease progression, which are influenced by body weight differences. Lastly, we demonstrated significant *Mecp2e1* genotype effects on measurements of fat mass, BMC, food intake, physical activity and energy expenditure in mice prior to the onset of weight gain, suggesting that metabolic disruptions due to MeCP2-e1 deficiency occur early in disease progression. Together, these results demonstrate a timeline of RTT-relevant phenotype progression in a mouse model of an actual RTT mutation that should be important for better understanding and treatment of human RTT.

Because of the complex MeCP2 mutant/wild-type mosaicism observed in *Mecp2* mutant female mice, the majority of RTT preclinical therapy trials in mice are performed only on *Mecp2* null male mice lacking MeCP2 in all cells (45–50). Reasons cited for only testing *Mecp2* null males include the obvious phenotype (death by 8–12 weeks) and the lack of confounding X-chromosome inactivation mosaicism. However, *MECP2* null mutations are not seen in human RTT patients, suggesting that *Mecp2* mutant mice designed from RTT-causing human mutations are more construct-relevant models (5,51–53). A variety of genetic models have been developed including whole exon deletions (9,10), specific DNA-binding domain deletions (14) and a variety of knock-in point and truncation mutations that model human mutations (42,54–58). The majority of these models develop deficits similar to those observed in RTT patients, including abnormal breathing, gait abnormalities, tremors, EEG abnormalities and in some cases cognitive deficits, social abnormalities and changes in anxiety behaviors (59). However, the complete loss of MeCP2 expression and the rapid and severe deterioration in the male models do not capture the delayed onset of symptoms and mosaic inactivation patterns of *MECP2* expression in RTT females. While death is the primary phenotype in male RTT mouse models, motor, respiratory, metabolic and severe gastrointestinal symptoms are more medically relevant to the variable range of phenotypes in female RTT patients, since > 70% of RTT women are still alive by age 45[35]. Our results demonstrating significant phenotypes of hind limb clasping, increased fat mass and motor deficits by 2 months of age in female MeCP2-e1-deficient mice therefore provide an important advancement to the existing literature.

Mecp2e1$^{-/+}$ females developed abnormal behaviors by 6–7 weeks of age, similar to previous observations in *Mecp2*$^{-/+}$ mutant females heterozygous for exons 3 and 4 deletion affecting both *Mecp2* isoforms (11,16,60). Motor deficits are among the most common and consistently observed phenotypes in male and female mouse (12,16,45,61–65) and rat (66–68) models of RTT. Both *Mecp2e1*$^{-/+}$ females and males develop progressive motor impairments over time. Female *Mecp2e1*$^{-/+}$ mutants show early motor impairments (8.6 weeks of age) in gait but not in rotarod. By later time points (ages 12–20 weeks) the motor phenotypes became fully evident in the mutant females in gait, beam-walking and rotarod impairments. The development of full motor phenotypes is delayed relative to *Mecp2*$^{bird-/+}$ females tested at the same ages in our previous study (16)

and more heavily influenced by body weight (Supplementary Material, Fig. S11). The increased body weight in *Mecp2e1*$^{-/+}$ females was a significant covariate or influenced the main effect of genotype on the majority of motor measures, indicating that the metabolic phenotypes in this model may exacerbate motor impairments.

Altered energy balance and metabolic measures have been observed in human RTT females (26–28). While dietary energy intake and fecal fat loss did not differ between RTT and controls, metabolic rates during sleep and quiet awake were significantly lower (26) and morning levels of leptin and adiponectin were elevated in RTT (17). In RTT females, involuntary motor movements can drive increased energy expenditure and may underlie some of the shifts in energy balance (26), but increased repetitive movements do not appear sufficient to increase total daily energy expenditure (27). RTT girls have lower levels of lean body mass but not body fat compared to healthy controls (27). However, when compared to disabled girls with other developmental disabilities that were matched for age, height, weight and BMI, RTT girls showed a lower percentage of lean body mass, higher absolute and relative fat mass and higher levels of energy expenditure (28). The altered body composition and energy balance observed in RTT suggest that changes in metabolism may contribute to the disorder and serve as a novel therapeutic target for RTT treatment.

Recent identification of mutations that enhance survival of *Mecp2*$^{-/y}$ males has established the link between *Mecp2* and lipid metabolism (33–35). Consistent with these findings, our results show that *Mecp2e1*$^{-/+}$ females at 12–14 weeks of age and *Mecp2e1*$^{-/y}$ males at 7–11 weeks of age display significant elevation in body fat percent and fat mass without significant elevation in weight on a C57BL6/J background. Interestingly, results most relevant to our studies show that *Mecp2*$^{-/y}$ mice on a 129 background are significantly heavier beginning at 7 weeks of age (34). Furthermore, while Kyle *et al*. showed reduced RER in *Mecp2*$^{-/y}$ mice in both the light and dark cycle (34), our results show that *Mecp2e1*$^{-/y}$ mice have elevated RER predominantly in the dark cycle. In terms of energy expenditure, we show that *Mecp2e1*$^{-/y}$ males have reduced dark and light phase energy expenditure even after adjusting for body weight or lean mass, consistent with reduced heat production during the light cycle for *Mecp2*$^{-/y}$ null mice on a 129 background as shown previously (34). The genetic background or genetic mutation difference of our *Mecp2e1*$^{-/y}$ mice on a C57BL6/J background may explain differences between studies, although the studies are consistent in showing metabolic alterations including decreased energy expenditure and increased mass in RTT mouse models. Bone defects in *Mecp2* null males were previously observed in *Mecp2* null mice (69), which is consistent with our findings in MeCP2-e1-deficient mice.

In support of a possible decreased energy expenditure in RTT mouse models across genetic backgrounds, previous metabolic analyses of RTT model mice carrying the B6.129P2(C)-Mecp2tm1.1Bird/J or 'Bird' null allele have shown that *Mecp2*$^{-/+}$ females have elevated body weight on 129 or C57BL6/J/129 mixed backgrounds (9,10,16,54,56). Similarly, genetic background clearly affects weight in *Mecp2* null (Bird) male mice as they were underweight on a C57BL6/J background while overweight on a 129 background (9,16) or mixed C57BL6/J/129 background (70). Interestingly, Kerr *et al*. also showed elevated weight in mice bearing the floxed, undeleted *Mecp2* (Bird) allele on a C57BL6/J/129 mixed background, suggesting an effect of the *Mecp2* 3'UTR on metabolic phenotype (71). Recently, Gigli *et al*. showed that *Mecp2*$^{-/y}$ male mice bred on a CD1 background have reduced weight at 6 weeks followed by significantly elevated adult weight, while CD1 *Mecp2*$^{-/+}$ females exhibit elevated weight starting at 17 weeks compared to wild-type littermates (72). Consistent with these findings, Torres-Andrade showed that *Mecp2* null (Bird) males on a mixed C57BL6/J/129 background were overweight by 7 weeks of age due to increased fat mass and that this was not due to increased food intake (73), again consistent with our results.

Conditional knockout experiments also have revealed common body weight effects from *Mecp2* deletion in specific neuronal subtypes. For example, *Mecp2* deletion in forebrain neurons led to significant weight gain compared to littermate controls at 13 weeks on the C57BL6/J background (74). Conditional *Mecp2* (Bird allele) knockout in hypothalamic neurons resulted in weight gain due to fat mass expansion in *Mecp2*$^{-/y}$ males by 7 weeks on a 129/Friend leukemia virus B (FVB) background (75). Also, *Mecp2*$^{-/y}$ males with a conditional deletion in only excitatory neurons became overweight by 6 weeks of age on a 129/FVB background (76). Conditional knockout of *Mecp2* in proopiomelanocortin (POMC) neurons resulted in increased body weight at 16 weeks in *Mecp2*$^{-/y}$ (Bird) males on a C57BL6/J background (77). Cumulatively, these experiments reveal the role of neuronal *Mecp2* expression in the regulation of weight and metabolism in mouse models.

Interestingly, in contrast to the male *Mecp2*$^{-/y}$ mice, *Mecp2e1*$^{-/+}$ female mice did not show clear changes in either energy expenditure or food intake prior to increases in body weight in the C57BL6/J background. These results suggest that there is a gene dosage effect on metabolic phenotypes in this RTT model that is observed prior to and somewhat independent from body weight differences. More subtle but non-significant differences in food intake or energy expenditure may be responsible for the weight gain in the female mutant mice, such as the increase in triglycerides observed in *Mecp2e1*$^{-/+}$ liver. More comprehensive studies of additional RTT mouse models across time points for both energy expenditure and lipidomic analysis are likely needed to determine the causes of weight gain and metabolic changes in *Mecp2*-deficient mice.

In conclusion, our results demonstrate that MeCP2-e1 deficiency is sufficient to cause hind-clasping, motor and metabolic phenotypes in both female and male mice. Increased body weight and fat mass were due to decreased energy expenditure, not increased food intake in MeCP2-e1-deficient male mice. Female mutant MeCP2-e1 mice showed increased fat mass and altered liver lipidomics, but not altered energy expenditure or food intake. This metabolic phenotype is consistent across multiple RTT models of different genetic mutations and backgrounds and is associated with neuronal deficiency of MeCP2. Understanding how neuronal MeCP2e1 deficiency interacts with metabolism during the molecular pathogenesis of disease progression in female RTT models is therefore of critical importance to the successful design of future therapies.

Materials and Methods

Breeding and Cross-fostering. *Mecp2-e1* heterozygous females (*Mecp2e1*$^{-/+}$) were maintained on a pure C57BL/6J background by breeding to wild-type C57BL/6J males (Jax strain 000664). To mitigate the impact of poor maternal care by *Mecp2e1*$^{-/+}$ dams, all pups were cross-fostered to CD1 foster dams within the first 48 h of birth. Briefly, *Mecp2e1*$^{-/+}$ females were paired with wild-type C57BL/6J males for 2 weeks. CD1 male and female mice were also paired over the same time period so that litters would

coincide. All males were then removed from the mating cages. Within the first 48 h of birth, the entire litter from *Mecp2e1*$^{-/+}$ dams was removed from their birth mother and placed with a CD1 dam that had given birth to a litter within the previous 24–48 h. All but two of the CD1 offspring were euthanized upon cross-fostering and all pups remained with the CD1 dam until weaning at PND 21. Mice were maintained in a conventional temperature controlled vivarium, with *ad libitum* access to food and water, with the lights on from 7 a.m.–7 p.m. Behavioral testing was conducted in adjacent testing rooms during the light phase of the circadian cycle. All experiments were conducted in accordance with the National Institutes of Health Guidelines for the Care and Use of Laboratory Animals. All procedures were approved by the Institutional Animal Care and Use Committee of the University of California, Davis and are covered under IACUC protocol #18881.

Developmental milestones (PNDs 6–20). Developmental milestones (78–80) were measured on PNDs 6, 8, 10, 12, 14, 16, 18 and 20 as previously described (16). All measures were conducted by an experimenter blind to genotype. Body weight and body length (nose to anus) were measured using a scale (grams) and ruler (cm). Pinnae detachment, ear detachment, eye opening, incisor eruption and fur development were each rated on a scale of 0 (not present) to 3 (fully present). Cliff avoidance was tested by placing each pup near the edge of a clipboard, gently nudging it towards the edge, and scoring avoidance on rating scale from 0 (no edge avoidance) to 3 (complete turning and backing away from the edge). Righting reflex was tested by placing each pup on its back, releasing it and measuring the time for it to fully flip over onto four paws for two trials on each developmental day. Failures to flip over in the righting test were recorded as a maximum score of 30 s. Grasping reflex was tested by brushing the forepaws with a cotton tipped applicator and rating the grasping reflex from 0 (none) to 3 (strong). Auditory startle was tested using a rating scale from 0 (no response) to 3 (large flinch and turn) in response to a finger snap near the pup's head. Bar holding was tested by placing each pup's front paws on a cotton tipped applicator stick and gently lifting up. Scoring consisted of a rating scale from 0 (immediate fall) to 3 (stay on and climb up). Level screen reflex was tested by placing each pup on a screen, gently pulling the tail and rating the level of resistance (0 = none to 3 = strong). Vertical screen reflex was tested by placing each pup on a screen at a 90° angle and rating the pup's ability to remain on the screen from 0 (immediate fall) to 3 (hold on and climb to top). Negative geotaxis was tested by placing each pup, facing downwards, on a screen angled at 45° from parallel and scored on a scale from 0 (no turning) to 3 (complete turning and climbing to the top of the screen).

Adult Behavioral Battery. Behaviors were assessed in young adult mice from PNDs 46–152 in females and PND 35–95 in males. Mice had free access to food and water and lights were maintained on a 12:12 h light/dark cycle, with all behavioral testing performed during the light portion of the cycle. All behavioral assessments were conducted by an experimenter blinded to genotype.

Body weight and Clasping Score (weekly PNDs 28–152 for females and PNDs 28–128 for males). Weekly body weights and hind limb clasping were assessed beginning from PND 28. Hind limb clasping was rated on a scale from 0 (no clasping behavior) to 5 (both hind limbs tucked in and abdomen contracted) (16,42).

Elevated Plus maze (PNDs 46–47 for females and PND 35 for males). Each mouse was individually placed in the center area of a black Plexiglas automated elevated plus maze (Med-Associates, St. Albans City, VT), under 300 lux illumination for a 5 min test session (79,81,82). The entries per arm, total entries and the time spent in each arm were recorded and compared between conditions (80).

Light ↔ Dark Exploration (PNDs 49–50 for females and PND 36 for males). The light ↔ dark exploration task was performed as previously described (79). Briefly, the automated photocell-equipped apparatus was made of two Plexiglas compartments separated by a partition with a small opening. One compartment was transparent and illuminated by an overhead light (400 lux). The other compartment was made of black Plexiglas and closed on top. Each mouse was placed into the center of the light compartment and allowed to freely explore for 10 min. The number of transitions between light and dark sides and time spent in each compartment were recorded and compared between conditions.

Open Field Exploration (PNDs 53–55 for females). Exploratory behavior was assessed in a novel open field as previously described (79). Each mouse was placed in an automated VersaMax Animal Activity Monitoring System (AccuScan Instruments, Columbus, OH) and allowed to freely explore for 30 min. The number of horizontal and vertical beam breaks was used as a measure of horizontal and vertical activity, respectively. Total distance traveled was used as a measure of total activity. Time spent in the center of the chamber compared to along the edges was recorded and compared between conditions.

Gait Analysis (PNDs 60–61 and 144 for females, PND 65 for males). On the day prior to analysis, all animals were habituated to restraint and paint application. On test day, each animal was restrained, and the front feet were painted with blue while the back feet were painted with red paint (Sargent Art 22-3350 Washable Paint Hazleton, PA). The mouse was then allowed to walk down a straight alleyway lined with drawing paper (Strathmore Neenah, WI). Colored footprints were analyzed for stride length (distance between successive forelimb and successive hind limb prints), hind-base (distance between the right and left hind prints), front-base (distance between right and left front prints) and paw separation (distance between the forepaw and hind paw placement) (83). Two to three footprints were analyzed per animal.

Accelerating Rotarod (PNDs 62–64 and 140–143 for females). Animals were given three trials per day with 1 h inter-trial intervals, repeated over 3 consecutive days (79,80). Each trial consisted of placing the animal on the rotarod apparatus (Ugo Basile Gemonio, VA, Italy mouse accelerating rotarod) and starting the rotation at 4 revolutions per min (rpm). After the mouse was successfully walking, the rotarod was accelerated from 4–40 rpm over 5 min (79). The latency to fall from the rotating beam to the flange on the floor of the apparatus was recorded for each animal. The trial was terminated in cases where the mouse clutched the beam without walking, for five consecutive turns, or a maximum of 300 s had elapsed (16,79,80).

Beam and Rod Walking (PNDs 88–92 and 152 for females, 60–64 and 95 for males). A beam-walking motor task was conducted as previously described (41). Square dowels of 59 cm in length were suspended 68 cm above a cushioned landing pad. A goal box at the end of the beam consisted of a 12 cm diameter cylinder to

provide motivation to cross the beam. Each mouse was placed at the end of the beam and the time to cross to the goal box on the other end was measured. On the day prior to testing, all animals were given four practice trials on the largest diameter square beam in order to become accustom to the procedure (83). On the test day, each animal was sequentially tested on three square beams (24 mm, 19 mm and 15 mm) and three round rods (17 mm, 12 mm and 9 mm). Testing sequence was based on presentations of decreasing diameter to present increasing levels of difficulty. Each mouse was given two trials on each beam, separated by ~30 min. The time to transverse the beam was recorded and averaged across the two trials for each beam. A maximum time of 60 s was assigned to individuals that failed to cross the beam in that duration. In the small number of cases where mice fell from the beam, a score of 60 s was assigned.

Social Approach (PNDs 74–78 in females). Sociability was assessed using the three-chambered social approach task as previously described (80,84,85). The testing apparatus consisted of three connected chambers made of white matte Plexiglas, separated by two sliding doors. Prior to testing, the subject mouse was placed in the empty center chamber with the doors closed for 5 min. Doors were then removed to allow free access to all three empty chambers for 10 min. Distance traveled and the number of entries into the two side chambers were automatically scored using three-point tracking with EthoVison XT tracking software (Noldus Information Technology Inc. Leesburg, VA). The mouse was then confined to the center chamber and a novel female 129Sv/ImJ mouse was placed in an inverted wire pencil cup in one chamber. An empty inverted wire pencil cup was simultaneously placed in the other chamber, to serve as the novel object. The partition doors were opened and the subject mouse was given free access to all three chambers for 10 min. Time spent and number of entries into each chamber, time spent sniffing the novel mouse and time the novel object and the total distance traveled were simultaneously scored using EithoVision XT (80,84,86).

Short-term Memory Novel Object Recognition and Object Location Recognition (PNDs 66–71 and 81–85 in females) and (PNDs 39–44 and 47–52 in males). Novel object recognition testing was performed as described previously (16,43,87). Briefly, all animals were handled for 2 min per day by the experimenter for 3 days. All animals were then habituated to the empty training arena for 10 min per day for 4 days. Distance travelled was recorded for each day of habituation and during training and testing. For the training session, each animal was placed into the arena with two identical objects for 10 min. A 5 min testing session occurred 60 min after training. For novel object recognition testing, one of the training objects was replaced with a novel object. For object location recognition testing, one of the training objects was placed in a novel location. Time spent exploring each object was scored by an experimenter blind to all conditions. Animals exploring less than 3 s total for both objects during training or testing were excluded from further analysis (88).

Energy expenditure, food intake and physical activity (PND 88 in females and PNDs 57–66 in males). CLAMS analysis was performed on five separate sub-cohorts of Mecp2e1 mutant and control female and male mice (Supplementary Material, Table S10). CLAMS analysis was performed on mice prior to significant changes in body weights and phenotypic scores between the two genotypes of each sex, hence the different time points in males and females. *Mecp2e1*$^{-/+}$ females (N = 11) and *Mecp2e1*$^{+/+}$ females (N = 12) were examined at PND 88 on day 0 of testing. *Mecp2e1*$^{-/y}$ males (N = 8) and *Mecp2e1*$^{+/y}$ control males (N = 9) were tested at PND 57–66 on day 0 of testing.

On day 0, mice were transferred to single chamber housing in CLAMS chambers (Columbus Instruments, Columbus, OH) for acclimation for 48 h, and then data was analyzed from the subsequent 48 h of CLAMS measurements. On day 1, mice in CLAMS chambers were transferred to a temperature controlled cabinet set to 24°C at 9:00 a.m. Data recording was initiated with the following settings: initial reference reading (2 min) +2 min/cage, reference settle time: 90 s, reference measure time 30 s, cage settle time: 90 s, cage measure time: 30 s and time to cycle for eight cages 18 min (3 readings/hr). Data including volume of oxygen consumed (VO_2), volume of carbon dioxide produced (VCO_2), mass of food consumed, total number of X-axis IR-Beam Breaks (X-Tot), number of Ambulatory (beam breaks in sequence) X-axis IR-Beam Breaks (X-amb), total number of Y-axis IR-Beam Breaks (Y-Tot), number of Ambulatory Y-axis IR-Beam Breaks (Y-amb) and number of Vertical (Rearing) Motions (Z-Tot) was acquired continuously for 4 days. RER was calculated as the ratio of carbon dioxide production/oxygen consumption. Heat production or energy expenditure is calculated from the equation, (Heat production = CV $*$ VO_2) where CV = 3.815 + 1.232 $*$ RER. Calorimeter analyzer calibration was completed in the morning prior to each 24 h measurement. A 0.50% CO_2 and 20.50% O_2 (balance nitrogen) calibration gas (Airgas, Sacramento, CA) and dry room air were used to calibrate the analyzers. At the start and end of the experiments, the performance of the entire calorimetry system was validated by bleeding a 20% CO_2 and 80% N_2 standard (Airgas, Sacramento, CA) into each calorimetry chamber at a regulated rate using an OxyVal gas infusion system (Columbus Instruments, Columbus, OH) and measuring recovery of CO_2 and dilution of O_2 in the chamber outflow.

DEXA analysis. On day 5, mice were removed from CLAMS chambers at 9 a.m. and euthanized by isoflurane inhalation prior to body composition analysis by DEXA. Percent fat, total fat mass, BMC, BMD, bone area and subject length were calculated from absorption of the two X-ray frequencies.

Untargeted complex lipid analysis of liver. Liver samples from *Mecp2e1*$^{-/+}$ females (N = 8) and *Mecp2e1*$^{+/+}$ females (N = 7) were flash frozen in RNA Later (Qiagen, Germantown, MD) immediately following the DEXA procedure for lipidomics. The untargeted lipidomics procedure began with lipid extraction from liver samples using methyl *tert*-butyl ether (MTBE) with the addition of internal standards, followed by ultra-high pressure liquid chromatography on a Waters CSH column, interfaced to a Q-TOF mass spectrometer (high resolution, accurate mass), with a 15 min total run time. Data are collected in both positive and negative ion mode and analyzed using Mass-Hunter (Agilent, Santa Clara, CA). Extraction of hepatic lipids was based on the "Matyash" method[36] (Matyash V, J. Lipid Research, 2008) which was subsequently modified. Briefly, extraction is carried out using a bi-phasic solvent system of cold methanol, MTBE and water. In more detail, cold methanol (225 µl) containing a mixture of odd chain and deuterated lipid internal standards [lysoPE(17:1), lysoPC(17:0), PC(12:0/13:0), PE(17:0/17:0), PG(17:0/17:0), sphingosine (d17:1), d_7-cholesterol, SM(17:0), C17 ceramide, d_3-palmitic acid, MG(17:0/0:0/0:0), DG(18:1/2:0/0:0), DG(12:0/12:0/0:0) and d_5-TG(17:0/17:1/17:0)] is added to a 20 µL sample aliquot, which is placed into a 1.5 mL Eppendorf tube, and the tube is vortexed for 10 s. Then, 750 µl of cold MTBE containing cholesterol ester (CE) (22:1) (internal standard) is added, followed by vortexing for 10 s and shaking for 6 min at 4°C. Phase separation is induced by adding 188 µl of mass

spec-grade water. After vortexing for 2 s, the sample was centrifuged at 14 000 rpm for 2 min. The upper organic phase was collected in two 300 µl aliquots. One was stored at −20°C as a backup and the other was evaporated to dryness in a SpeedVac. Dried extracts were resuspended using a mixture of methanol/toluene (9:1, v/v) (60 µL) containing an internal standard [12-[[(cyclohexylamino) carbonyl]amino]-dodecanoic acid (CUDA)] used as a quality control.

LC/MS parameters. The LC/QTOFMS analyses were performed using an Agilent 1290 Infinity LC system (G4220A binary pump, G4226A autosampler and G1316C Column Thermostat) coupled to either an Agilent 6530 (positive ion mode) or an Agilent 6550 mass spectrometer equipped with an ion funnel (iFunnel) (negative ion mode). Lipids were separated on an Acquity UPLC CSH C18 column (100 × 2.1 mm; 1.7 µm) maintained at 65°C at a flow rate of 0.6 mL/min. Solvent pre-heating (Agilent G1316) was used. The mobile phases consisted of 60:40 acetonitrile:water with 10 mM ammonium formate and 0.1% formic acid (A) and 90:10 propan-2-ol:acetonitrile with 10 mM ammonium formate and 0.1% formic acid. The gradient was established as follows: 0 min 85% (A); 0–2 min 70% (A); 2–2.5 min 52% (A); 2.5–11 min 18% (A); 11–11.5 min 1% (A); 11.5–12 min 1% (A); 12–12.1 min 85% (A); 12.1–15 min 85% (A). A sample volume of 3 µl was used for the injection. Sample temperature was maintained at 4°C in the auto-sampler.

The quadrupole/time-of-flight (QTOF) mass spectrometers were operated with electrospray ionization (ESI) performing a full scan in the mass range *m/z* 65–1700 in positive (Agilent 6530, equipped with a JetStreamSource) and negative (Agilent 6550, equipped with a dual JetStream Source) modes producing both unique and complementary spectra. Instrument paramaters were as follows: (positive mode) Gas Temp 325°C, Gas Flow 8 l/min, Nebulizer 35 psig, Sheath Gas 350°C, Sheath Gas Flow 11, Capillary Voltage 3500 V, Nozzle Voltage 1000V, Fragmentor 120V and Skimmer 65V. Data (both profile and centroid) were collected at a rate of two scans per second. Gas Temp 200°C, Gas Flow 14 l/min, Fragmentor 175V, along with the other parameters were identical for both negative and positive ion mode. For the 6530 QTOF, a reference solution generating ions of 121.050 and 922.007 *m/z* in positive mode and 119.036 and 966.0007 *m/z* in negative mode was used for continuous mass correction. For the 6550, the reference solution was introduced via a dual spray ESI, with the same ions and continuous mass correction. Samples were injected (1.7 uls in positive mode and 5 uls in negative ion mode) with a needle wash for 20 s (wash solvent was isopropanol). The valve was switched back and forth during the run for washing, which has been shown to be essential for reducing carryover of less polar lipids.

Untargeted Lipidomics Data Analysis. For data processing, the MassHunter software was used, and a unique ID was given to each lipid based on its retention time and exact mass (RT_mz). This allows the report of peak areas/heights or concentration of lipids based on the use of particular internal standards. Lipids are identified based on their unique MS/MS fragmentation patterns using in-house software, Lipidblast. Using complex lipid class-specific internal standards this approach was used to quantify > 400 lipid species including the following: mono-, di- and triacylglycerols, glycerophospholipids, sphingolipids, cholesterol esters, ceramides and fatty acids. Peak area/heights (intensity) data was recorded from the MS/MS data.

Metaboanalyst analysis. MetaboAnalyst 4.0 was used for analysis of QTOF-MS/MS peak intensity data. Settings for MetaboAnalyst (http://www.metaboanalyst.ca/) analysis were as follows: data filtering using interquantile range, sample normalization by sum, data transformation using log and Pareto scaling. Sample groups were considered to be unpaired. For fold change (FC) analysis, Mecp2e1$^{-/+}$ (MUTANT) peak heights over Mecp2e1$^{+/+}$ wild-type peak heights with a cutoff of log2 FC at > 1.0 or < 1.0 was used.

Statistical analyses of the data. Male and female developmental milestone data were analyzed separately. Continuous outcomes (body weight, body length and average righting reflex time) were analyzed using linear mixed effects models, including fixed effects for genotype, time and litter size (number of pups); the interaction genotype x time interaction; and random intercepts for mouse and litter (nlme and lsmeans R packages). Categorical ratings of pinnae detachment, eye opening, incisor eruption and fur development were analyzed using mixed effects Cox proportional hazards models of the time to full development; these models included fixed effects for genotype and litter size and a random slope for litter (coxme and car R packages). Categorical ratings of cliff avoidance, auditory startle, negative geotaxis, bar holding, vertical screen and level screen were analyzed using global F tests from regression models for ordinal data via cumulative link (mixed) models (clmm function from Ordinal R package) with fixed effects for genotype, time and litter size as well as the genotype x time interaction and random intercepts for mouse and litter. For males auditory startle ratings on the first time of assessment were not variable enough for inclusion in the model. For level screen scores, there was insufficient variability in scores for males beyond day 14 and for females beyond day 12 so only the first four or three time points were analyzed, respectively.

Post-weaning weight was analyzed separately for each sex using a linear mixed effects model, including fixed effects for genotype, time, genotype x time interaction and random effect of mouse. Benjamini–Hochberg corrected *post-hoc* comparisons were made for each time point. The development of significant hind limb clasping in the mutant mice was assessed for each time point where at least one animal showed a non-zero clasping score. At each time point examined, the number of animals with non-zero clasping scores was assessed using a binomial test (R package binom, with the binom.confint function with two-sided test) to assess if clasping was significantly greater than zero (no clasping) with an overall Benjamini–Hochberg correction across time points.

All other behavioral analyses included parametric independent, two-tailed t-tests or ANOVA models with Benjamini–Hochberg-corrected multiple *post-hoc* tests. Repeated measures tasks were accessed using a mixed model repeated measures ANOVA with a repeated measure and genotype and fostering as factors. All analyses were conducted using R, version 3.3.1 (89) or prism version 7. Linear mixed effects modeling was conducted using the R package lme4, version 1.1-12 (90), or nlme, version 3.1-131.1 (91) with lsmeans, version 2.27-61 (92), mixed effects Cox proportional hazards modeling was conducted using the R package coxme, version 2.2-5 (93) and mixed effects proportional odds logistic regression modeling was conducted using the R packages ordinal, version 2015.6-28 (94).

For CLAMS and DEXA analysis, all data are expressed as mean ± SEM unless otherwise indicated. Differences within a group were evaluated by t-test while differences between

genotypes and sexes were evaluated using a two-way ANOVA (95). *Post-hoc* analysis was carried out using a Tukey's honest significant difference test. For energy expenditure data, ANCOVA was used with either body weight or lean mass as a covariate in the model.

Supplementary Material

Supplementary Material is available at *HMG* online.

Acknowledgements

A.V.C., D.H.Y., J.M.L. and J.N.C. designed experiments and wrote the manuscript. A.V.C. and M.P. conducted behavioral experiments. B.D.J. conducted statistical analyses. A.V.C., A.C., A.N. and D.H.Y. assisted with behavioral scoring and data analysis. J.L.R. and J.R. performed the CLAMS and DEXA analysis. Metabolomics analysis was conducted by West Coast Metabolomics Center. The EE ANCOVA analysis was provided by the NIDDK Mouse Metabolic Phenotyping Centers (MMPC, www.mmpc.org) using their Energy Expenditure Analysis page (http://www.mmpc.org/shared/regression.aspx). Thank you to Heather Boyle and the animal care staff at UC Davis for colony management, breeding and cross-fostering. This research was also supported by the UC Davis MIND Institute Intellectual and Developmental Disabilities Research Center (U54HD079125).

Conflict of Interest statement. None declared.

Funding

National Institutes of Health (T32MH073124-06 to A.V.C., 3RO1NS 081913-11S1 to J.M.L., 5R01NS081913-14 to J.M.L., U54HD079125 to J.N.C., J.M.L., and B.D.J., UL1TR000002 to B.D.J., 1R01NS085709 to JNC); the Brain and Behavior Foundation (NARSAD Young Investigator Grant to A.V.C.) and the International Rett Syndrome Foundation to J.M.L. B.D.J. is supported by UL1 TR001860. Metabolomics analysis was supported by a University of California (UC) Davis pilot grant through the West Coast Metabolomics Center (NIH U24 DK097154). The National Institute of Diabetes and Digestive Kidney Disease (NIDDK) Mouse Metabolic Phenotyping Center is supported through grants DK076169 and DK115255. We are grateful for the technical support and/or services provided to our research by the UC Davis, Mouse Metabolic Phenotyping Centers, Energy Balance Exercise and Behavior Core, which is supported by U24 DK092993 (RRID:SCR_015364).

References

1. Mnatzakanian, G.N., Lohi, H., Munteanu, I., Alfred, S.E., Yamada, T., MacLeod, P.J.M., Jones, J.R., Scherer, S.W., Schanen, N.C., Friez, M.J. *et al.* (2004) A previously unidentified MECP2 open reading frame defines a new protein isoform relevant to Rett syndrome. *Nat. Genet.*, **36**, 339–341.
2. Gianakopoulos, P.J., Zhang, Y., Pencea, N., Orlic-Milacic, M., Mittal, K., Windpassinger, C., White, S.J., Kroisel, P.M., Chow, E.W.C., Saunders, C.J. *et al.* (2012) Mutations in MECP2 exon 1 in classical Rett patients disrupt MECP2_e1 transcription, but not transcription of MECP2_e2. *Am. J. Med. Genet. Part B Neuropsychiatr. Genet.*, **159B**, 210–216.
3. Saunders, C.J., Minassian, B.E., Chow, E.W.C., Zhao, W. and Vincent, J.B. (2009) Novel exon 1 mutations in MECP2 implicate isoform MeCP2-e1 in classical Rett syndrome. *Am. J. Med. Genet. Part A*, **149**, 1019–1023.
4. Kriaucionis, S. and Bird, A. (2004) The major form of MeCP2 has a novel N-terminus generated by alternative splicing. *Nucleic Acids Res.*, **32**, 1818–1823.
5. Yasui, D.H., Gonzales, M.L., Aflatooni, J.O., Crary, F.K., Hu, D.J., Gavino, B.J., Golub, M.S., Vincent, J.B., Schanen, N.C., Olson, C.O. *et al.* (2014) Mice with an isoform-ablating Mecp2 exon 1 mutation recapitulate the neurologic deficits of Rett syndrome. *Hum. Mol. Genet.*, **23**, 1–12.
6. Itoh, M., Tahimic, C.G.T., Ide, S., Otsuki, A., Sasaoka, T., Noguchi, S., Oshimura, M., Goto, Y.I. and Kurimasa, A. (2012) Methyl CpG-binding protein isoform MeCP2-e2 is dispensable for Rett syndrome phenotypes but essential for embryo viability and placenta development. *J. Biol. Chem.*, **287**, 13859–13867.
7. Braunschweig, D., Simcox, T., Samaco, R.C. and LaSalle, J.M. (2004) X-Chromosome inactivation ratios affect wild-type MeCP2 expression within mosaic Rett syndrome and Mecp2-/+ mouse brain. *Hum. Mol. Genet.*, **13**, 1275–1286.
8. Young, J.I. and Zoghbi, H.Y. (2004) X-Chromosome inactivation patterns are unbalanced and affect the phenotypic outcome in a mouse model of Rett syndrome. *Am. J. Hum. Genet.*, **74**, 511–520.
9. Guy, J., Hendrich, B., Holmes, M., Martin, J.E. and Bird, A. (2001) A mouse Mecp2-null mutation causes neurological symptoms that mimic Rett syndrome. *Nat. Genet.*, **27**, 322–326.
10. Chen, R.Z., Akbarian, S., Tudor, M. and Jaenisch, R. (2001) Deficiency of methyl-CpG binding protein-2 in CNS neurons results in a Rett-like phenotype in mice. *Nat. Genet.*, **27**, 327–331.
11. Samaco, R.C., McGraw, C.M., Ward, C.S., Sun, Y., Neul, J.L. and Zoghbi, H.Y. (2013) Female Mecp2(+/-) mice display robust behavioral deficits on two different genetic backgrounds providing a framework for pre-clinical studies. *Hum. Mol. Genet.*, **22**, 96–109.
12. Santos, M., Silva-Fernandes, A., Oliveira, P., Sousa, N. and Maciel, P. (2007) Evidence for abnormal early development in a mouse model of Rett syndrome. *Genes Brain Behav.*, **6**, 277–286.
13. Picker, J.D., Yang, R., Ricceri, L. and Berger-Sweeney, J. (2006) An altered neonatal behavioral phenotype in Mecp2 mutant mice. *Neuroreport*, **17**, 541–544.
14. Pelka, G.J., Watson, C.M., Radziewic, T., Hayward, M., Lahooti, H., Christodoulou, J. and Tam, P.P.L. (2006) Mecp2 deficiency is associated with learning and cognitive deficits and altered gene activity in the hippocampal region of mice. *Brain*, **129**, 887–898.
15. Cobolli Gigli, C., Scaramuzza, L., Gandaglia, A., Bellini, E., Gabaglio, M., Parolaro, D., Kilstrup-Nielsen, C., Landsberger, N. and Bedogni, F. (2016) MeCP2 related studies benefit from the use of CD1 as genetic background. *PLoS One*, **11**, e0153473.
16. Vogel Ciernia, A., Pride, M.C., Durbin-Johnson, B., Noronha, A., Chang, A., Yasui, D.H., Crawley, J.N. and LaSalle, J.M. (2017) Early motor phenotype detection in a female mouse model of Rett syndrome is improved by cross-fostering. *Hum. Mol. Genet.*, **26**, 1839–1854.
17. Blardi, P., De Lalla, A., D'Ambrogio, T., Vonella, G., Ceccatelli, L., Auteri, A. and Hayek, J. (2009) Long-term plasma levels of leptin and adiponectin in Rett syndrome. *Clin. Endocrinol. (Oxf).*, **70**, 706–709.

18. Borghi, E., Borgo, F., Severgnini, M., Savini, M.N., Casiraghi, M.C. and Vignoli, A. (2017) Rett syndrome: a focus on gut microbiota. *Int. J. Mol. Sci.*, **18**, 344.
19. Leoncini, S., De Felice, C., Signorini, C., Pecorelli, A., Durand, T., Valacchi, G., Ciccoli, L. and Hayek, J. (2011) Oxidative stress in Rett syndrome: natural history, genotype, and variants. *Redox Rep.*, **16**, 145–153.
20. De Felice, C., Della Ragione, F., Signorini, C., Leoncini, S., Pecorelli, A., Ciccoli, L., Scalabrì, F., Marracino, F., Madonna, M., Belmonte, G. *et al.* (2014) Oxidative brain damage in Mecp2-mutant murine models of Rett syndrome. *Neurobiol. Dis.*, **68**, 66–77.
21. De Felice, C., Signorini, C., Leoncini, S., Pecorelli, A., Durand, T., Valacchi, G., Ciccoli, L. and Hayek, J. (2012) The role of oxidative stress in Rett syndrome: an overview. *Ann. N. Y. Acad. Sci.*, **1259**, 121–135.
22. Cronk, J.C., Derecki, N.C., Ji, E., Xu, Y., Lampano, A.E., Smirnov, I., Baker, W., Norris, G.T., Marin, I., Coddington, N. *et al.* (2015) Methyl-CpG binding protein 2 regulates microglia and macrophage gene expression in response to inflammatory stimuli. *Immunity*, **42**, 679–691.
23. O'Driscoll, C.M., Lima, M.P., Kaufmann, W.E. and Bressler, J.P. (2015) Methyl CpG binding protein 2 deficiency enhances expression of inflammatory cytokines by sustaining NF-κB signaling in myeloid derived cells. *J. Neuroimmunol.*, **283**, 23–29.
24. Cortelazzo, A., De Felice, C., Guerranti, R., Signorini, C., Leoncini, S., Pecorelli, A., Zollo, G., Landi, C., Valacchi, G., Ciccoli, L. *et al.* (2014) Subclinical inflammatory status in Rett syndrome. *Mediators Inflamm.*, **2014**, 1–13.
25. Pecorelli, A., Cervellati, F., Belmonte, G., Montagner, G., Waldon, P., Hayek, J., Gambari, R. and Valacchi, G. (2016) Cytokines profile and peripheral blood mononuclear cells morphology in Rett and autistic patients. *Cytokine*, **77**, 180–188.
26. Motil, K.J., Schultz, R., Brown, B., Glaze, D.G. and Percy, A.K. (1994) Altered energy balance may account for growth failure in Rett syndrome. *J. Child Neurol.*, **9**, 315–319.
27. Motil, K.J., Schultz, R.J., Wang, W.W. and Glaze, D.G. (1998) Increased energy expenditure associated with repetitive involuntary movement does not contribute to growth failure in girls with Rett syndrome. *J. Pediatr.*, **132**, 228–233.
28. Platte, P., Jaschke, H., Herbert, C. and Korenke, G.C. (2011) Increased resting metabolic rate in girls with Rett syndrome compared to girls with developmental disabilities. *Neuropediatrics*, **42**, 179–182.
29. Budden, S.S., Myer, E.C. and Butler, I.J. (1990) Cerebrospinal fluid studies in the Rett syndrome: biogenic amines and beta-endorphins. *Brain Dev.*, **12**, 81–84.
30. Haas, R.H., Light, M., Rice, M. and Barshop, B.A. (1995) Oxidative metabolism in Rett syndrome: 1. Clinical studies. *Neuropediatrics*, **26**, 90–94.
31. Shulyakova, N., Andreazza, A.C., Mills, L.R. and Eubanks, J.H. (2017) Mitochondrial dysfunction in the pathogenesis of Rett syndrome: implications for mitochondria-targeted therapies. *Front. Cell. Neurosci.*, **11**, 58.
32. Jin, L.-W., Horiuchi, M., Wulff, H., Liu, X.-B., Cortopassi, G.A., Erickson, J.D. and Maezawa, I. (2015) Dysregulation of glutamine transporter SNAT1 in Rett syndrome microglia: a mechanism for mitochondrial dysfunction and neurotoxicity. *J. Neurosci.*, **35**, 2516–2529.
33. Buchovecky, C.M., Turley, S.D., Brown, H.M., Kyle, S.M., McDonald, J.G., Liu, B., Pieper, A.A., Huang, W., Katz, D.M., Russell, D.W. *et al.* (2013) A suppressor screen in Mecp2 mutant mice implicates cholesterol metabolism in Rett syndrome. *Nat. Genet.*, **45**, 1013–1020.
34. Kyle, S.M., Saha, P.K., Brown, H.M., Chan, L.C. and Justice, M.J. (2016) MeCP2 co-ordinates liver lipid metabolism with the NCoR1/HDAC3 corepressor complex. *Hum. Mol. Genet.*, **25**, 3029–3041.
35. Lopez, A.M., Chuang, J.-C., Posey, K.S. and Turley, S.D. (2017) Suppression of brain cholesterol synthesis in male Mecp2-deficient mice is age dependent and not accompanied by a concurrent change in the rate of fatty acid synthesis. *Brain Res.*, **1654**, 77–84.
36. Villani, C., Sacchetti, G., Bagnati, R., Passoni, A., Fusco, F., Carli, M. and Invernizzi, R.W. (2016) Lovastatin fails to improve motor performance and survival in methyl-CpG-binding protein2-null mice. *Elife*, **5**, 1–14.
37. Leonard, H., Cobb, S. and Downs, J. (2017) Clinical and biological progress over 50 years in Rett syndrome. *Nat. Rev. Neurol.*, **13**, 37–51.
38. Ricciardi, S., Boggio, E.M., Grosso, S., Lonetti, G., Forlani, G., Stefanelli, G., Calcagno, E., Morello, N., Landsberger, N., Biffo, S. *et al.* (2011) Reduced AKT/mTOR signaling and protein synthesis dysregulation in a Rett syndrome animal model. *Hum. Mol. Genet.*, **20**, 1182–1196.
39. Li, Y., Wang, H., Muffat, J., Cheng, A.W., Orlando, D.A., Lovén, J., Kwok, S.-M., Feldman, D.A., Bateup, H.S., Gao, Q. *et al.* (2013) Global transcriptional and translational repression in human-embryonic-stem-cell-derived Rett syndrome neurons. *Cell Stem Cell*, **13**, 446–458.
40. Filosa, S., Pecorelli, A., D'Esposito, M., Valacchi, G. and Hajek, J. (2015) Exploring the possible link between MeCP2 and oxidative stress in Rett syndrome. *Free Radic. Biol. Med.*, **88**, 81–90.
41. Justice, M.J., Buchovecky, C.M., Kyle, S.M. and Djukic, A. (2013) A role for metabolism in Rett syndrome pathogenesis: new clinical findings and potential treatment targets. *Rare Dis. (Austin, Tex.)*, **1**, 1–6.
42. Yasui, D.H., Gonzales, M.L., Aflatooni, J.O., Crary, F.K., Hu, D.J., Gavino, B.J., Golub, M.S., Vincent, J.B., Schanen, N.C., Olson, C.O. *et al.* (2014) Mice with an isoform-ablating Mecp2 exon 1 mutation recapitulate the neurologic deficits of Rett syndrome. *Hum. Mol. Genet.*, **23**, 2447–2458.
43. Vogel-Ciernia, A. and Wood, M.A. (2014) Examining object location and object recognition memory in mice. *Curr. Protoc. Neurosci.*, **2014**, 8.31.1–8.31.17.
44. Jin, L.-W., Horiuchi, M., Wulff, H., Liu, X.-B., Cortopassi, G.A., Erickson, J.D. and Maezawa, I. (2015) Dysregulation of glutamine transporter SNAT1 in Rett syndrome microglia: a mechanism for mitochondrial dysfunction and neurotoxicity. *J. Neurosci.*, **35**, 2516–2529.
45. Nag, N. and Berger-Sweeney, J.E. (2007) Postnatal dietary choline supplementation alters behavior in a mouse model of Rett syndrome. *Neurobiol. Dis.*, **26**, 473–480.
46. Doppler, E., Rockenstein, E., Ubhi, K., Inglis, C., Mante, M., Adame, A., Crews, L., Hitzl, M., Moessler, H. and Masliah, E. (2008) Neurotrophic effects of Cerebrolysin in the Mecp2308/Y transgenic model of Rett syndrome. *Acta Neuropathol.*, **116**, 425–437.
47. Kline, D.D., Ogier, M., Kunze, D.L. and Katz, D.M. (2010) Exogenous brain-derived neurotrophic factor rescues synaptic dysfunction in Mecp2-null mice. *J. Neurosci.*, **30**, 5303–5310.
48. Tropea, D., Giacometti, E., Wilson, N.R., Beard, C., McCurry, C., Fu, D.D., Flannery, R., Jaenisch, R. and Sur, M. (2009) Partial

reversal of Rett syndrome-like symptoms in MeCP2 mutant mice. *Proc. Natl. Acad. Sci. USA.*, **106**, 2029–2034.
49. Roux, J.-C., Dura, E., Moncla, A., Mancini, J. and Villard, L. (2007) Treatment with desipramine improves breathing and survival in a mouse model for Rett syndrome. *Eur. J. Neurosci.*, **25**, 1915–1922.
50. Ogier, M., Wang, H., Hong, E., Wang, Q., Greenberg, M.E. and Katz, D.M. (2007) Brain-derived neurotrophic factor expression and respiratory function improve after ampakine treatment in a mouse model of Rett syndrome. *J. Neurosci.*, **27**, 10912–10917.
51. Moretti, P., Bouwknecht, J.A., Teague, R., Paylor, R. and Zoghbi, H.Y. (2005) Abnormalities of social interactions and home-cage behavior in a mouse model of Rett syndrome. *Hum. Mol. Genet.*, **14**, 205–220.
52. Tarquinio, D.C., Hou, W., Neul, J.L., Kaufmann, W.E., Glaze, D.G., Motil, K.J., Skinner, S.A., Lee, H.-S. and Percy, A.K. (2015) The changing face of survival in Rett syndrome and MECP2-related disorders. *Pediatr. Neurol.*, **53**, 402–411.
53. Matyash, V., Liebisch, G., Kurzchalia, T.V., Shevchenko, A. and Schwudke, D. (2008) Lipid extraction by methyl-tert-butyl ether for high-throughput lipidomics. *J. Lipid Res.*, **49**, 1137–1146.
54. Shahbazian, M., Young, J., Yuva-Paylor, L., Spencer, C., Antalffy, B., Noebels, J., Armstrong, D., Paylor, R. and Zoghbi, H. (2002) Mice with truncated MeCP2 recapitulate many Rett syndrome features and display hyperacetylation of histone H3. *Neuron*, **35**, 243–254.
55. Brown, K., Selfridge, J., Lagger, S., Connelly, J., De Sousa, D., Kerr, A., Webb, S., Guy, J., Merusi, C., Koerner, M.V. *et al.* (2016) The molecular basis of variable phenotypic severity among common missense mutations causing Rett syndrome. *Hum. Mol. Genet.*, **25**, 558–570.
56. Goffin, D., Allen, M., Zhang, L., Amorim, M., Wang, I.-T.J., Reyes, A.-R.S., Mercado-Berton, A., Ong, C., Cohen, S., Hu, L. *et al.* (2012) Rett syndrome mutation MeCP2 T158A disrupts DNA binding, protein stability and ERP responses. *Nat. Neurosci.*, **15**, 274–283.
57. Brendel, C., Belakhov, V., Werner, H., Wegener, E., Gärtner, J., Nudelman, I., Baasov, T. and Huppke, P. (2011) Readthrough of nonsense mutations in Rett syndrome: evaluation of novel aminoglycosides and generation of a new mouse model. *J. Mol. Med. (Berl).*, **89**, 389–398.
58. Jentarra, G.M., Olfers, S.L., Rice, S.G., Srivastava, N., Homanics, G.E., Blue, M., Naidu, S. and Narayanan, V. (2010) Abnormalities of cell packing density and dendritic complexity in the MeCP2 A140V mouse model of Rett syndrome/X-linked mental retardation. *BMC Neurosci.*, **11**, 11–19.
59. Katz, D.M., Berger-Sweeney, J.E., Eubanks, J.H., Justice, M.J., Neul, J.L., Pozzo-Miller, L., Blue, M.E., Christian, D., Crawley, J.N., Giustetto, M. *et al.* (2012) Preclinical research in Rett syndrome: setting the foundation for translational success. *Dis. Model. Mech.*, **5**, 733–745.
60. Stearns, N.A., Schaevitz, L.R., Bowling, H., Nag, N., Berger, U.V. and Berger-Sweeney, J. (2007) Behavioral and anatomical abnormalities in Mecp2 mutant mice: a model for Rett syndrome. *Neuroscience*, **146**, 907–921.
61. Schaevitz, L.R., Gómez, N.B., Zhen, D.P. and Berger-Sweeney, J.E. (2013) MeCP2 R168X male and female mutant mice exhibit Rett-like behavioral deficits. *Genes Brain Behav.*, **12**, 732–740.
62. Garg, S.K., Lioy, D.T., Cheval, H., McGann, J.C., Bissonnette, J.M., Murtha, M.J., Foust, K.D., Kaspar, B.K., Bird, A. and Mandel, G. (2013) Systemic delivery of MeCP2 rescues behavioral and cellular deficits in female mouse models of Rett syndrome. *J. Neurosci.*, **33**, 13612–13620.
63. Jugloff, D.G.M., Vandamme, K., Logan, R., Visanji, N.P., Brotchie, J.M. and Eubanks, J.H. (2008) Targeted delivery of an Mecp2 transgene to forebrain neurons improves the behavior of female Mecp2-deficient mice. *Hum. Mol. Genet.*, **17**, 1386–1396.
64. Kondo, M., Gray, L.J., Pelka, G.J., Christodoulou, J., Tam, P.P.L. and Hannan, A.J. (2008) Environmental enrichment ameliorates a motor coordination deficit in a mouse model of Rett syndrome—Mecp2 gene dosage effects and BDNF expression. *Eur. J. Neurosci.*, **27**, 3342–3350.
65. Stearns, N.A., Schaevitz, L.R., Bowling, H., Nag, N., Berger, U.V. and Berger-Sweeney, J. (2007) Behavioral and anatomical abnormalities in Mecp2 mutant mice: a model for Rett syndrome. *Neuroscience*, **146**, 907–921.
66. Veeraragavan, S., Wan, Y.W., Connolly, D.R., Hamilton, S.M., Ward, C.S., Soriano, S., Pitcher, M.R., McGraw, C.M., Huang, S.G., Green, J.R. *et al.* (2015) Loss of MeCP2 in the rat models regression, impaired sociability and transcriptional deficits of Rett syndrome. *Hum. Mol. Genet.*, **25**, 3284–3302.
67. Wu, Y., Zhong, W., Cui, N., Johnson, C.M., Xing, H., Zhang, S. and Jiang, C. (2016) Characterization of Rett syndrome-like phenotypes in Mecp2-knockout rats. *J. Neurodev. Disord.*, **8**, 1–12.
68. Patterson, K.C., Hawkins, V.E., Arps, K.M., Mulkey, D.K. and Olsen, M.L. (2015) MeCP2 deficiency results in robust Rett-like behavioural and motor deficits in male and female rats. *Hum. Mol. Genet.*, **25**, 3303–3320.
69. O'Connor, R.D., Zayzafoon, M., Farach-Carson, M.C. and Schanen, N.C. (2009) Mecp2 deficiency decreases bone formation and reduces bone volume in a rodent model of Rett syndrome. *Bone*, **45**, 346–356.
70. Pitcher, M.R., Ward, C.S., Arvide, E.M., Chapleau, C.A., Pozzo-Miller, L., Hoeflich, A., Sivaramakrishnan, M., Saenger, S., Metzger, F. and Neul, J.L. (2013) Insulinotropic treatments exacerbate metabolic syndrome in mice lacking MeCP2 function. *Hum. Mol. Genet.*, **22**, 2626–2633.
71. Kerr, B., Alvarez-saavedra, M., Sáez, M.A., Saona, A. and Young, J.I. (2008) Defective body-weight regulation, motor control and abnormal social interactions in Mecp2 hypomorphic mice. *Hum. Mol. Genet.*, **17**, 1707–1717.
72. Gigli, C.C., Scaramuzza, L., Gandaglia, A., Bellini, E., Gabaglio, M., Parolaro, D., Kilstrup-Nielsen, C., Landsberger, N. and Bedogni, F. (2016) MeCP2 related studies benefit from the use of CD1 as genetic background. *PLoS One*, **11**, 1–14.
73. Torres-Andrade, R., Moldenhauer, R., Gutierrez-Bertín, N., Soto-Covasich, J., Mancilla-Medina, C., Ehrenfeld, C. and Kerr, B. (2014) The increase in body weight induced by lack of methyl CpG binding protein-2 is associated with altered leptin signalling in the hypothalamus. *Exp. Physiol.*, **99**, 1229–1240.
74. Gemelli, T., Berton, O., Nelson, E.D., Perrotti, L.I., Jaenisch, R. and Monteggia, L.M. (2006) Postnatal loss of Methyl-CpG binding protein 2 in the forebrain is sufficient to mediate behavioral aspects of Rett syndrome in mice. *Biol. Psychiatry*, **59**, 468–476.
75. Fyffe, S.L., Neul, J.L., Samaco, R.C., Chao, H.-T., Ben-Shachar, S., Moretti, P., McGill, B.E., Goulding, E.H., Sullivan, E., Tecott, L.H. *et al.* (2008) Deletion of Mecp2 in Sim1-expressing neurons reveals a critical role for MeCP2 in feeding behavior, aggression, and the response to stress. *Neuron*, **59**, 947–958.

76. Meng, X., Wang, W., Lu, H., He, L.J., Chen, W., Chao, E.S., Fiorotto, M.L., Tang, B., Herrera, J.A., Seymour, M.L. *et al*. (2016) Manipulations of MeCP2 in glutamatergic neurons highlight their contributions to Rett and other neurological disorders. *Elife*, **5**, 1–21.
77. Wang, X., Lacza, Z., Sun, Y.E. and Han, W. (2014) Leptin resistance and obesity in mice with deletion of methyl-CpG-binding protein 2 (MeCP2) in hypothalamic pro-opiomelanocortin (POMC) neurons. *Diabetologia*, **57**, 236–245.
78. Fox, W.M. (1965) Reflex-ontogeny and behavioural development of the mouse. *Anim. Behav.*, **13**, 234–241.
79. Brielmaier, J., Matteson, P.G., Silverman, J.L., Senerth, J.M., Kelly, S., Genestine, M., Millonig, J.H., DiCicco-Bloom, E. and Crawley, J.N. (2012) Autism-relevant social abnormalities and cognitive deficits in engrailed-2 knockout mice. *PLoS One*, **7**, 40–42.
80. Yang, M., Bozdagi, O., Scattoni, M.L., Wohr, M., Roullet, F.I., Katz, A.M., Abrams, D.N., Kalikhman, D., Simon, H., Woldeyohannes, L. *et al*. (2012) Reduced excitatory neurotransmission and mild autism-relevant phenotypes in adolescent Shank3 null mutant mice. *J. Neurosci.*, **32**, 6525–6541.
81. Yang, M., Lewis, F.C., Sarvi, M.S., Foley, G.M. and Crawley, J.N. (2015) 16p11.2 Deletion mice display cognitive deficits in touchscreen learning and novelty recognition tasks. *Learn. Mem.*, **22**, 622–632.
82. Kazdoba, T.M., Hagerman, R.J., Zolkowska, D., Rogawski, M.A. and Crawley, J.N. (2016) Evaluation of the neuroactive steroid ganaxolone on social and repetitive behaviors in the BTBR mouse model of autism. *Psychopharmacology (Berl)*, **233**, 309–323.
83. Carter, R.J., Morton, J. and Dunnett, S.B. (2001) Motor coordination and balance in rodents. *Curr. Protoc. Neurosci.*, **Chapter 8**, Unit 8.12.
84. Yang, M., Silverman, J.L. and Crawley, J.N. (2011) Automated three-chambered social approach task for mice. *Curr. Protoc. Neurosci.*, **Chapter 8**, Unit 8.26.
85. Silverman, J.L., Pride, M.C., Hayes, J.E., Puhger, K.R., Butler-Struben, H.M., Baker, S. and Crawley, J.N. (2015) GABAB receptor agonist R-Baclofen reverses social deficits and reduces repetitive behavior in two mouse models of autism. *Neuropsychopharmacology*, **40**, 2228–2239.
86. Nadler, J.J., Moy, S.S. and Dold, G. (2004) Automated apparatus for quantitation of social approach behaviors in mice. *Genes Brain Behav.*, **3**, 303–314.
87. Vogel-Ciernia, A., Matheos, D.P., Barrett, R.M., Kramár, E.A., Azzawi, S., Chen, Y., Magnan, C.N., Zeller, M., Sylvain, A., Haettig, J. *et al*. (2013) The neuron-specific chromatin regulatory subunit BAF53b is necessary for synaptic plasticity and memory. *Nat. Neurosci.*, **16**, 552–561.
88. Vogel-Ciernia, A. and Wood, M.A. (2013) Neuron-specific chromatin remodeling: a missing link in epigenetic mechanisms underlying synaptic plasticity, memory, and intellectual disability disorders. *Neuropharmacology*, **0**, 18–27.
89. R Development Core Team (2011) R: a language and environment for statistical computing. R Foundation for Statistical Computing, Vienna, Austria. URL http://www.R-project.org/.
90. Bates, D., Mächler, M., Bolker, B. and Walker, S. (2015) Fitting linear mixed-effects models using lme4. *J. Stat. Softw.*, **67**, 1–48.
91. Pinheiro, J., Bates, D., DebRoy, S. and Sarker, D. (2018) nlme: linear and nonlinear mixed effects models., R package version 3.0.
92. Lenth, R.V. (2016) Least-squares means: the R package lsmeans. *J. Stat. Softw.*, **69**, 1–33.
93. Therneau, T.M. (2015) Mixed effects Cox models., *R pakage version* 2.2–10.
94. Christensen, R.H.B. (2015) Ordinal–regression models for ordinal data., *R package version* 2018.4–19.
95. Assaad, H.I., Hou, Y., Zhou, L., Carroll, R.J. and Wu, G. (2015) Rapid publication-ready MS-Word tables for two-way ANOVA. *Springerplus*, **4**, 33.